International Journal of Solids and Structures 176–177 (2019) 68–85

Contents lists available at ScienceDirect

International Journal of Solids and Structures

journal homepage: www.elsevier.com/locate/ijsolstr

Group-theoretic vibration analysis of double-layer cable nets of D_{4h} symmetry

Alphose Zingoni

Department of Civil Engineering, University of Cape Town, Rondebosch 7701, Cape Town, South Africa

ARTICLE INFO

Article history:
Received 16 January 2019
Revised 20 April 2019
Accepted 20 May 2019
Available online 21 May 2019

Keywords:
Cable net
Vibration
Symmetry
Group theory
Eigenvalue problem
Mode shape

ABSTRACT

Shallow cable nets may be coupled into multi-layer configurations that are stiffer and stronger than single-layer configurations. In a previous study, group theory was used to investigate double-layer cable nets of D_{4h} symmetry by reference to a 32-node case study, revealing key insights on their vibration characteristics. In this paper, and as an extension of the previous work, we present a rigorous group-theoretic formulation for the computation of natural frequencies and mode shapes of double-layer cable nets of D_{4h} symmetry, by reference to the same case study. The analysis reveals the existence of transverse-extension modes that are unique to coupled cable-net configurations, at the same time demonstrating the substantial computational benefits of the group-theoretic procedure. A numerical example is considered in order to illustrate how the eigenvalues and eigenmodes of the problem are actually calculated, providing further insights on the vibration behaviour of the cable net.

1. Introduction

Cable nets may be formed by prestressing a set of cables running in one direction against another set of cables running in the perpendicular direction, with the two systems of cables being curved in opposite directions. Such a system is very capable of resisting external loads, with the stiffness of the structure being very much a function of the tensile forces in the individual cables.

Cable nets find application as lightweight roofing systems for long spans (Irvine, 1981; Szabo and Kollar, 1984; Vilnay, 1990). They are usually shallow, with the vertical rise (or fall) of the net being relatively small in comparison with the lateral dimensions of the net. For present purposes, we will consider cable nets as shallow if the rise-to-span ratio is less than 1/5. For such shallow nets, the reference plane for transverse motions may be taken as horizontal. In the present study, which follows on earlier work (Zingoni, 2018), we are interested in the small transverse motions (i.e. vertical vibrations) of shallow cable nets, where one set of cables is assumed to run in the x coordinate direction and the other set of cables is assumed to run in the y coordinate direction, with the transverse direction being vertical and denoted by the z axis.

Following the assumptions of the earlier study (Zingoni, 2018), the motion of the cable net is represented by discrete masses located at the intersections of the cables, and the cables are assumed to have tensile stiffness but no mass. All the mass of the cables (and any additional mass due to fittings) is lumped at the nodes of the cable net. Lumped-parameter modelling is, of course, not as exact as distributed-parameter modelling, but for the purposes of gaining important insights on the key features of the vibration response of the system, it is adequate. Other assumptions that we will make are that the tensions in the cables are relatively large, and the transverse displacements of the cable net remain relatively small during vibration, so that the magnitudes of the tensile forces in the cables do not change appreciably during the motion. Moreover, the friction between the cables at their intersections is considered to be negligible, so that the tensile force in a given cable remains practically constant throughout its length. These linear assumptions can be realised to a very good degree in many practical situations.

Here, we are interested in cable nets that possess symmetry properties, which are quite abundant in practice. Symmetry has an influence on the static and kinematic behaviour of structures (Zingoni et al., 1995; Kangwai et al., 1999; Kangwai and Guest, 1999, 2000; Fowler and Guest, 2000; Guest and Fowler, 2007; Chen et al., 2015), and special methods employed to analyse this behaviour include those based on graph theory and its variants (Kaveh and Rahami, 2004; Kaveh and Nikbakht, 2007; Kaveh and Koohestani, 2008; Kaveh and Nikbakht, 2010; Chen and Feng, 2016), and those based on group theory (Healey, 1988; Zlokovic, 1989; Ikeda and Murota, 1991; Healey and Treacy, 1991; Zingoni, 1996; Mohan and Pratap, 2004; Zingoni, 2005; Zingoni, 2008; Chen and Feng, 2012; Zingoni, 2012; Harth and Michelberger, 2016). Group theory is particularly suited to the study of physical systems possessing multiple symmetry properties, and has been particularly fruitful in physics and chemistry (Weyl, 1932;

E-mail address: alphose.zingoni@uct.ac.za

https://doi.org/10.1016/j.ijsolstr.2019.05.020
0020-7683/

Wigner, 1959; Hamermesh, 1962; Schonland, 1965). Within engineering mechanics, group theory has been extensively employed to simply the analysis of problems of the statics, kinematics, vibration, stability and bifurcation of structures (Zingoni, 2009). Such studies have included, among others, previous work of the author on the vibration of single-layer cable nets (Zingoni, 1996) and double-layer space grids (Zingoni, 2005) of C_{nv} symmetry, and on the determination of natural frequencies for rectilinear spring-mass dynamic systems that can be transformed into equivalent C_{nv} systems (Zingoni, 2008). Group-theoretic ideas have been exploited by other investigators to tackle the problem of the forced vibration response of spring-mass models of C_{nv} symmetry (Kaveh and Jahanmohammadi, 2008), and the linear vibration analysis of shells with dihedral symmetry (Mohan and Pratap, 2002). Group theory has also been shown to provide valuable insights on structural behaviour (Zingoni, 2014; Chen et al., 2015), before any numerical computations are performed. Furthermore, group-theoretic formulations have been developed for numerical applications such as the finite-difference analysis of plates (Zingoni, 2012) and the finite-element analysis of skeletal and continuum structures (Zingoni, 1996, 2005). Symmetry is not always easy to identify in complex structures, so some studies have been directed towards developing procedures for the automatic recognition of symmetry (Suresh and Sirpotdar, 2006; Zingoni, 2012; Chen et al., 2017, 2018).

Some remarks on the validity of the physical model adopted here are in order. Although cable nets are generally considered to be geometrically non-linear structures and usually analysed as such (Siev, 1963; Otto, 1966; Buchholdt et al., 1968), their load-deformation response may be nearly linear under certain conditions, permitting a linear analysis. Even if this is not exactly the case, essentially linear techniques may be used to overcome the non-linear effects (Calladine, 1982; Pellegrino and Calladine, 1984; Vilnay and Rogers, 1990). In our present treatment, the modelling of cable-net behaviour has been kept very simple, even within the context of linear theory itself, in order to keep the focus on symmetry and its effects. The intention is not to present a refined model of cable-net behaviour; rather, it is to study the effects and implications of symmetry, for which a simple physical model of the cable net suffices. In any case, the cable net is assumed to be shallow and highly tensioned, with the amplitude of the free vertical vibrations remaining small throughout, conditions under which the behaviour of the cable net is reasonably linear.

The vibration of single-layer cable nets with horizontal projections of C_{2v} and C_{4v} symmetries (i.e. the symmetries of a rectangle and a square respectively) have been studied in a previous paper (Zingoni, 1996). Group theory enabled vibration modes having coincident frequencies to be identified, and other predictions (such as the existence of stationary nodes and nodal lines) to be made. In the current work, we employ group theory to study the vibration characteristics of double-layer cable nets belonging to the symmetry group D_{4h}. Such cable nets may be formed by coupling (in the vertical direction) two single-layer cable nets of C_{4v} symmetry. Of interest here are extensible couplings whose axial stiffness may be modelled by vertical springs. Coupling of shallow cable nets into double-layer configurations offers the possibility of altering the load-carrying and dynamic characteristics of single-layer systems in a beneficial way. However, the higher-order symmetry of the D_{4h} configuration complicates the vibration response of the cable net. Group theory becomes particularly useful for unravelling the complexities and better understanding the dynamic response.

Like the vibrating particles of a layered crystal structure with orthorhombic (D_{2h}), tetragonal (D_{4h}) or cubic (O_h) symmetry, layered cable nets of D_{nh} symmetry exhibit transverse extensional modes (i.e. expansion and contraction of the vertical distance between layers) which are irrelevant in the case of single-layer cable nets and other single-layer structures that have been studied in the past. In the case of double-layer cable nets of present interest, the spring-like coupling between the two layers permits the upper and lower layers of the cable net to move independently of each other, thus doubling the total number of system degrees of freedom, in comparison with single-layer cable nets (or rigidly connected double-layer cable nets whose layers move up and down together).

It is the occurrence of these additional extensional modes (or "breathing" modes) that distinguishes the present study from the previous one (Zingoni, 1996). Group theory is expected to reveal new insights specific to D_{nh} cable-net configurations. Indeed, for the problem of the vibration of double-layer cable nets of D_{4h} symmetry, such insights have already been reported in the first part of the current work (Zingoni, 2018). These have included the type of symmetries to be expected of the various vibration modes, the number of modes that will exhibit a given type of symmetry, the existence of pairs of modes of the same natural frequency, and the nature of the symmetry associated with such paired modes.

The present paper is a continuation of the work on double-layer cable nets of D_{4h} symmetry. Having gained some qualitative insights in the first paper (Zingoni, 2018), we will now turn our attention to computational aspects. We will present the group-theoretic formulation of the eigenvalue problem, and using the results for subspace basis vectors that were presented in the first paper (Zingoni, 2018), we will show how symmetry-adapted flexibility matrices for all ten subspaces are obtained, and how subspace eigenvalues (i.e. natural frequencies of the cable net) readily follow.

The structure of the rest of the paper is as follows. In Section 2, we outline the linear theory governing the response of the cable net, and present the equations of motion for the upper and lower layers of the net. In Section 3, we present a brief description of the group-theoretic procedure as applied to vibration analysis. In Section 4, after describing the layout and symmetry properties of the double-layer cable net that will form the subject of the rest of the paper, we summarise key results for symmetry-adapted freedoms (basis vectors) for the various subspaces of the problem, as derived in the companion paper (Zingoni, 2018). These are central to the derivations in Section 5, where basis vectors are used to generate the symmetry-adapted flexibility matrices for all ten subspaces of the problem. Symmetry-adapted mass matrices are presented in Section 6. In Section 7, the general procedure for the calculation of eigenvalues and eigenvectors is explained, and in Section 8, a numerical example is considered, to illustrate how the natural frequencies and mode shapes of the cable net are actually calculated. The final section summarises the findings and conclusions of the paper.

2. Conventional formulation of the problem

We assume the double-layer cable net lies in the *xyz* Cartesian-coordinate reference system. For a given layer (top or bottom), let us denote the constant horizontal component of the cable force in the lth cable of the x-orientated cables (numbering ξ) by $H_{x,l}$, the constant horizontal component of the cable force in the jth cable of the y-orientated cables (numbering η) by $H_{y,j}$, the horizontal spacing of the x-orientated cables by a, the horizontal spacing of the y-orientated cables by b, the vertical coordinate of the equilibrium position of node $\{j,\ l\}$ of the net by $z_{j,l}$, the vertical load at node $\{j,\ l\}$ by $P_{j,l}$, and the concentrated mass at node $\{j,\ l\}$ by $m_{j,l}$. Furthermore, let us distinguish the top and bottom layers of the cable net by the superscripts t and b respectively. The stiffness of the spring connecting the top and bottom nodes of the cable net at the intersection $\{j,\ l\}$ will be denoted by $k_{j,l}$.

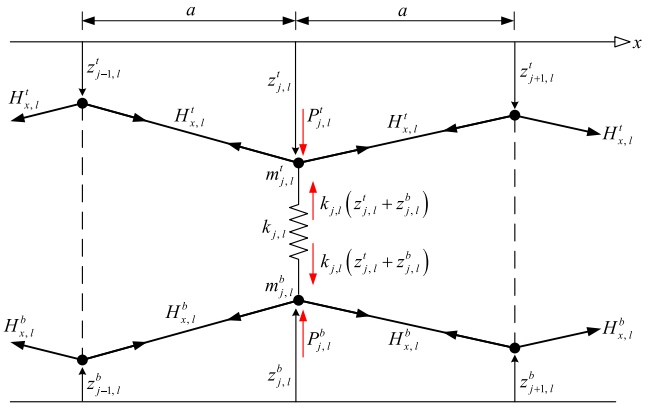

Fig. 1. Forces at top and bottom nodes of cable-net intersection $\{j,\ l\}$ when the masses are in their equilibrium positions.

Fig. 1 is a view in the *xz* vertical plane, showing the forces at the top and bottom nodes of cable intersection $\{j,\ l\}$. Notice that for the top layer, the nodal displacements and nodal loads are considered positive when acting downwards, whereas for the bottom layer, nodal displacements and nodal loads are considered positive when acting upwards. This convention is consistent with the group-theoretic convention proposed by the author in some of his earlier work (Zingoni, 2008, 1996, 2005), where the centre of symmetry or plane of symmetry is taken as the origin or the reference plane, and displacements or forces are considered positive if away or towards the centre of symmetry or plane of symmetry. In the present problem, the reference plane for the system is the horizontal *xy* plane of symmetry that lies midway between the two cable-net layers. We take the direction towards the plane of symmetry as the positive direction (i.e. downwards for the top-layer nodes, and upwards for the bottom-layer nodes). Applied to the double-layer cable net, this novel convention allows us to take advantage of horizontal mirror symmetry more efficiently. The view in the *yz* vertical plane would be similar, except that the cable forces become $H_{y,j}$, the *z* parameters assume the values for the *y* direction, and the cable-spacing parameter becomes *b*.

By reference to the figure, the following relations, which are statements of the condition of vertical equilibrium at nodes $\{j,\ l\}$ $(j=1,\ 2,\ \ldots,\ \eta;\ \ l=1,\ 2,\ \ldots,\ \xi)$ of the top and bottom layers of the cable net, may be written down:

$$\frac{H^t_{x,\,l}}{a}\left(2z^t_{j,\,l}-z^t_{j-1,\,l}-z^t_{j+1,\,l}\right)+\frac{H^t_{y,\,j}}{b}\left(2z^t_{j,\,l}-z^t_{j,\,l-1}-z^t_{j,\,l+1}\right)+k_{j,\,l}\left(z^t_{j,\,l}+z^b_{j,\,l}\right)-P^t_{j,\,l}=0 \tag{1a}$$

$$\frac{H^b_{x,\,l}}{a}\left(2z^b_{j,\,l}-z^b_{j-1,\,l}-z^b_{j+1,\,l}\right)+\frac{H^b_{y,\,j}}{b}\left(2z^b_{j,\,l}-z^b_{j,\,l-1}-z^b_{j,\,l+1}\right)+k_{j,\,l}\left(z^t_{j,\,l}+z^b_{j,\,l}\right)-P^b_{j,\,l}=0 \tag{1b}$$

Note that for the top node, we have resolved the forces in the upward direction (i.e. we have taken "upwards" as positive), while for the bottom node, we have resolved the forces in the downward direction (i.e. we have taken "down" as positive). The two equations are coupled through the $k_{j,\,l}$ terms that contain displacements of both layers.

Let us denote the small-amplitude vertical vibrations of the cable-net nodes by $v_{j,\,l}$. At node $\{j,\ l\}$, the displacement $v_{j,\,l}$ due to vibration is measured from the equilibrium position of the node. Similar to the convention adopted for $z_{j,\,l}$, for the top layer of the cable net, $v_{j,\,l}$ is considered positive when acting downwards, while for the bottom layer, $v_{j,\,l}$ is considered positive when acting upwards. Consistent with the assumption of linear behaviour, the intervals *a* and *b* do not change significantly during vibration, and, as already stated, $H_{x,\,l}$ and $H_{y,\,j}$ also remain practically constant. Adapting Equations (1), the equations of motion for nodes $\{j,\ l\}$ of the top and bottom layers of the cable net may therefore be written as

$$\frac{H^t_{x,\,l}}{a}\left[2(z^t_{j,\,l}+v^t_{j,\,l})-(z^t_{j-1,\,l}+v^t_{j-1,\,l})-(z^t_{j+1,\,l}+v^t_{j+1,\,l})\right]+\frac{H^t_{y,\,j}}{b}\left[2(z^t_{j,\,l}+v^t_{j,\,l})-(z^t_{j,\,l-1}+v^t_{j,\,l-1})-(z^t_{j,\,l+1}+v^t_{j,\,l+1})\right]+k_{j,\,l}\left\{\left(z^t_{j,\,l}+v^t_{j,\,l}\right)+\left(z^b_{j,\,l}+v^b_{j,\,l}\right)\right\}-P^t_{j,\,l}+m^t_{j,\,l}\ddot{v}^t_{j,\,l}=0 \tag{2a}$$

$$\frac{H^b_{x,\,l}}{a}\left[2(z^b_{j,\,l}+v^b_{j,\,l})-(z^b_{j-1,\,l}+v^b_{j-1,\,l})-(z^b_{j+1,\,l}+v^b_{j+1,\,l})\right]+\frac{H^b_{y,\,j}}{b}\left[2(z^b_{j,\,l}+v^b_{j,\,l})-(z^b_{j,\,l-1}+v^b_{j,\,l-1})-(z^b_{j,\,l+1}+v^b_{j,\,l+1})\right]+k_{j,\,l}\left\{\left(z^t_{j,\,l}+v^t_{j,\,l}\right)+\left(z^b_{j,\,l}+v^b_{j,\,l}\right)\right\}-P^b_{j,\,l}+m^b_{j,\,l}\ddot{v}^b_{j,\,l}=0 \tag{2b}$$

where for each layer, $\ddot{v}_{j,\,l}$ is the acceleration of mass $m_{j,\,l}$, and the last term on the left-hand side represents the inertial force acting on the mass.

Making use of Eqs. (1) to simplify Eqs. (2), we obtain

$$\frac{H^t_{x,\,l}}{a}\left(2v^t_{j,\,l}-v^t_{j-1,\,l}-v^t_{j+1,\,l}\right)+\frac{H^t_{y,\,j}}{b}\left(2v^t_{j,\,l}-v^t_{j,\,l-1}-v^t_{j,\,l+1}\right)+k_{j,\,l}\left(v^t_{j,\,l}+v^b_{j,\,l}\right)+m^t_{j,\,l}\ddot{v}^t_{j,\,l}=0 \tag{3a}$$

$$\frac{H^b_{x,\,l}}{a}\left(2v^b_{j,\,l}-v^b_{j-1,\,l}-v^b_{j+1,\,l}\right)+\frac{H^b_{y,\,j}}{b}\left(2v^b_{j,\,l}-v^b_{j,\,l-1}-v^b_{j,\,l+1}\right)+k_{j,\,l}\left(v^t_{j,\,l}+v^b_{j,\,l}\right)+m^b_{j,\,l}\ddot{v}^b_{j,\,l}=0 \tag{3b}$$

In our formulation of the vibration problem, we will use the flexibility approach (rather than the stiffness method), in view of its conceptual advantages. The cable-net system has a total of $2\eta\xi$ nodes (i.e. $\eta\xi$ nodes per layer). The associated flexibility coefficients can readily be calculated on the basis of Equations (1), as the deflections that ensue at each of the $2\eta\xi$ nodes of the cable net, when a unit vertical load is applied at node $\{r,\ s\}$ $(r=1,\ 2,\ \ldots,\ \eta;\ \ s=1,\ 2,\ \ldots,\ \xi)$ of layer i $(i=1,\ 2)$ while all other nodes are unloaded.

We set up, using Eqs. (1), a system of $2\eta\xi$ simultaneous equations in $2\eta\xi$ unknowns (i.e. the $z^t_{j,\,l}$ and $z^b_{j,\,l}$), whose right-hand sides are all zeros except when $j=r$ and $l=s$ in the layer in which the unit load is applied, where $P^t_{j,\,l}=P^t_{r,\,s}=1$ or $P^b_{j,\,l}=P^b_{r,\,s}=1$ (depending on whether the unit load is placed in the top layer or the bottom layer). This system is then solved for the $z^t_{j,\,l}$ and $z^b_{j,\,l}$. The procedure is repeated with the unit vertical load at another node of the cable net, until all $2\eta\xi$ nodes of the layer have been subjected, one node at a time, to the unit vertical load. In this way, all the $4\eta^2\xi^2$ flexibility coefficients of the linear-elastic net can be generated. Unfortunately the procedure can be computationally very challenging if the parameters η and ξ are very large. Hence the need for computational simplifications.

The group-theoretic approach decomposes the vector space of the cable-net problem into a number of independent subspaces spanned by symmetry-adapted variables, within which flexibility matrices are of dimensions much smaller than $2\eta\xi\times 2\eta\xi$. This enables us to obtain the natural frequencies of vibration and mode shapes of the cable net much more conveniently.

3. The group-theoretic procedure in brief

The first step of a group-theoretic analysis consists in identifying the symmetry elements, and hence the symmetry group *G* of

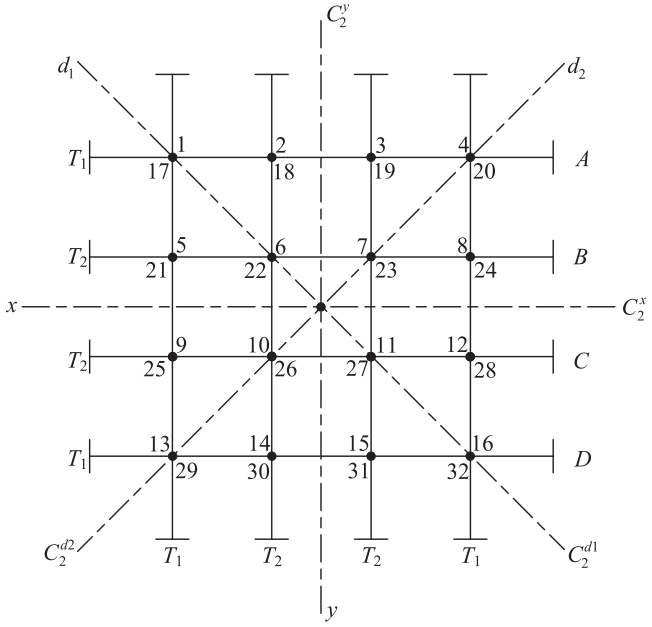

Fig. 2. Plan view of 32-node double-layer cable net of D_{4h} symmetry.

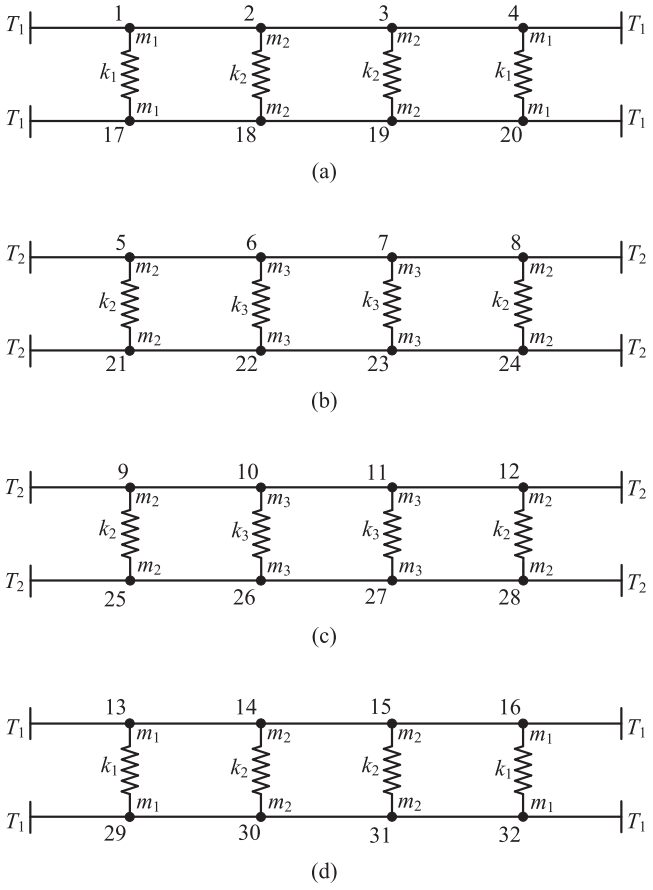

Fig. 3. Vertical sections of the 32-node double-layer cable net (refer to labels in plan view of Fig. 2): (a) section *A*; (b) section *B*; (c) section *C*; (d) section *D*.

a given physical problem. An idempotent $P^{(i)}$ corresponding to a given irreducible representation $R^{(i)}$ of the symmetry group, when applied on arbitrary vectors of the space V of the problem, has the property of nullifying every vector which does not belong to the subspace $S^{(i)}$ associated with $R^{(i)}$ (Zingoni et al., 1995; Zlokovic, 1989; Zingoni, 1996, 2005, 2015). Thus, the operator $P^{(i)}$ selects all vectors belonging to the subspace $S^{(i)}$, and therefore acts as a *projection operator* (Hamermesh, 1962) of the subspace $S^{(i)}$. Idempotents of groups D_{2h} and D_{4h} were given in the preceding paper (Zingoni, 2018).

In vibration problems, applying an idempotent to each of the arbitrary functions describing the motions of a system with n degrees of freedom gives the symmetry-adapted functions for the corresponding subspace, from which a set of r ($r<<n$) independent basis vectors spanning that subspace may readily be written down. This procedure was illustrated in detail in the preceding paper (Zingoni, 2018), where all subspace basis vectors for the D_{4h} cable net were derived.

For a given subspace of the decomposed problem, the basis vectors take the place of the normal degrees of freedom in a conventional vibration analysis, and are used to derive the symmetry-adapted flexibility matrix for the subspace. The symmetry-adapted mass matrix may also be readily written down, as this is simply made up of the values of the masses at the locations of the basis vectors. This allows a smaller eigenvalue problem to be set up for each subspace.

Solving the eigenvalue problem for a given subpace (which is of dimension r), we obtain the eigenvalues of the subspace which, very importantly, are also the eigenvalues of the original problem (Hamermesh, 1962). In this way, all the eigenvalues (or natural frequencies) of the original problem are obtained by solving a series of smaller eigenvalues problems, all independently of each other. In this way, the group-theoretic approach affords a significant saving in computational effort.

4. The double-layer cable net of D_{4h} symmetry

4.1. Layout and symmetry properties

Let us consider the 32-node double-layer cable net that was introduced in the earlier paper (Zingoni, 2018). For ease of reference, we will repeat the description of that cable net. Fig. 2 shows a horizontal projection of the cable net, with the top-layer nodes numbered 1 to 16 and the bottom-layer nodes numbered 17 to 32. The cable net is, of course, curved in 3-dimensional space, but being very shallow, it may be approximated as two layers of cable nodes in parallel horizontal planes, as shown in the vertical sections of Fig. 3. The overall configuration belongs to symmetry group D_{4h}.

In Fig. 2, the principal rotation axis C_n is vertical and passes through the centre of the diagram; it contains the centre of symmetry of the whole configuration, which is located midway between the two layers of the cable net. The vertical C_n axis is associated with the rotation symmetry operations $\{C_4,\ C_4^{-1},\ C_2\}$. The horizontal reflection plane associated with the symmetry operation σ_h is located at the level of the centre of symmetry of the configuration. The combination of rotations about the C_n axis and reflection in the horizontal central plane gives rise to the rotary-reflection operations $\{S_4,\ S_4^{-1},\ S_2\}$, the last of these being equivalent to the inversion operation i.

The four vertical reflection planes associated with the symmetry operations $\{\sigma_x, \sigma_y, \sigma_{d1}, \sigma_{d2}\}$ are indicated by the coordinate axes $\{x,\ y\}$ and the diagonal axes $\{d_1, d_2\}$ as shown. These four vertical planes also contain the nonprincipal C_2 rotation axes $\{C_2^x,\ C_2^y,\ C_2^{d1},\ C_2^{d2}\}$ which are all horizontal and pass through the centre of symmetry. For a more detailed description of the symmetry elements of group D_{4h}, reference may be made to the preceding paper (Zingoni, 2018).

The cables are assumed to carry prestressing forces of magnitude T_1 or T_2. In plan, the arrangement of cable forces conforms to C_{4v} symmetry (as is clear from Fig. 2). In elevation, pairs of cables lying in the same vertical plane have the same prestress force

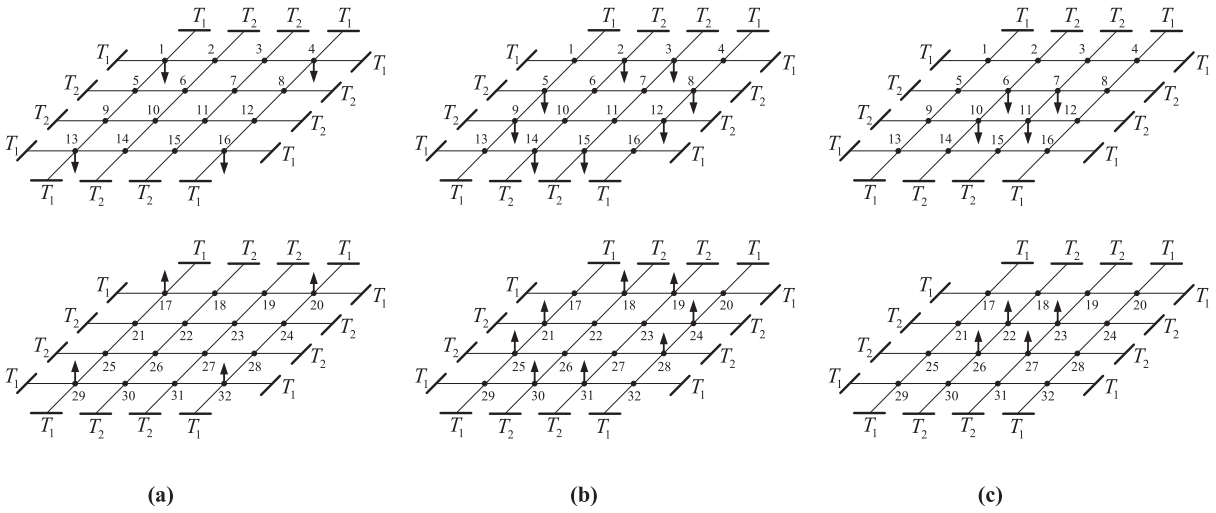

Fig. 4. Unit vertical forces applied in accordance with the coordinates of the basis vectors for subspace $S^{(1)}$: (a) Set of unit forces associated with $\Phi_1^{(1)}$; (b) Set of unit forces associated with $\Phi_2^{(1)}$; (c) Set of unit forces associated with $\Phi_3^{(1)}$. (For interpretation of the references to color in this figure, the reader is referred to the web version of this article.)

(see Fig. 3). Thus the overall pattern of prestressing also conforms to the D_{4h} symmetry of the structural configuration. If group D_{4h} is to be applicable to the vibration analysis, then the pattern of prestressing, which is an internal property of the cable net, must have the full D_{4h} symmetry of the structural layout. However, external loads that are applied at the nodes do not have to conform to any particular symmetry group, as any set of arbitrary external loads can always be decomposed into symmetry-adapted loads, and the components so obtained allocated to their respective subspaces (Zingoni et al., 1995).

The symmetry operations of group D_{4h}, when applied on the nodal positions 1 to 32 of the double-layer cable net, yield three permutation sets: corner nodes {1, 4, 13, 16, 17, 20, 29, 32}, mid-side nodes {2, 3, 5, 8, 9, 12, 14, 15, 18, 19, 21, 24, 25, 28, 30, 31}, and centre nodes {6, 7, 10, 11, 22, 23, 26, 27}. Consistent with the requirements of D_{4h} symmetry, each node of a given permutation set will be modelled with the same mass, and the vertical members coupling the nodes of a given permutation set will also be assigned the same stiffness. The masses and coupling stiffnesses for the three sets of nodes are denoted by $\{m_1, m_2, m_3\}$ and $\{k_1, k_2, k_3\}$ respectively, as illustrated in Fig. 3.

4.2. Symmetry-adapted freedoms

As shown in the preceding paper (Zingoni, 2018), application of the idempotents of symmetry group D_{4h} to the vector space of the 32-node double-layer cable net (which is spanned by the degrees of freedom $v_1, v_2, \ldots, v_{32}$ representing the vertical motions of the masses at the cable nodes) decomposes the vector space into 12 subspaces which are spanned by symmetry-adapted freedoms as basis vectors. Here is a summary of the results, which form the basis of the derivations in Section 5:

Basis vectors for subspace $S^{(1)}$

$$\Phi_1^{(1)} = v_1 + v_4 + v_{13} + v_{16} + v_{17} + v_{20} + v_{29} + v_{32} \tag{4a}$$

$$\Phi_2^{(1)} = v_2 + v_3 + v_5 + v_8 + v_9 + v_{12} + v_{14} + v_{15} + v_{18} + v_{19} + v_{21} + v_{24} + v_{25} + v_{28} + v_{30} + v_{31} \tag{4b}$$

$$\Phi_3^{(1)} = v_6 + v_7 + v_{10} + v_{11} + v_{22} + v_{23} + v_{26} + v_{27} \tag{4c}$$

Basis vector for subspace $S^{(2)}$

$$\Phi_1^{(2)} = v_2 - v_3 - v_5 + v_8 + v_9 - v_{12} - v_{14} + v_{15} + v_{18} - v_{19} - v_{21} + v_{24} + v_{25} - v_{28} - v_{30} + v_{31} \tag{5}$$

Basis vector for subspace $S^{(3)}$

$$\Phi_1^{(3)} = v_2 + v_3 - v_5 - v_8 - v_9 - v_{12} + v_{14} + v_{15} + v_{18} + v_{19} - v_{21} - v_{24} - v_{25} - v_{28} + v_{30} + v_{31} \tag{6}$$

Basis vectors for subspace $S^{(4)}$

$$\Phi_1^{(4)} = v_1 - v_4 - v_{13} + v_{16} + v_{17} - v_{20} - v_{29} + v_{32} \tag{7a}$$

$$\Phi_2^{(4)} = v_2 - v_3 + v_5 - v_8 - v_9 + v_{12} - v_{14} + v_{15} + v_{18} - v_{19} + v_{21} - v_{24} - v_{25} + v_{28} - v_{30} + v_{31} \tag{7b}$$

$$\Phi_3^{(4)} = v_6 - v_7 - v_{10} + v_{11} + v_{22} - v_{23} - v_{26} + v_{27} \tag{7c}$$

Basis vectors for subspace $S^{(5A)}$

$$\Phi_1^{(5A)} = \Phi_1^{(5)} = v_1 - v_{16} - v_{17} + v_{32} \tag{8a}$$

$$\Phi_2^{(5A)} = \Phi_6^{(5)} = v_6 - v_{11} - v_{22} + v_{27} \tag{8b}$$

$$\Phi_3^{(5A)} = \Phi_2^{(5)} + \Phi_5^{(5)} = v_2 + v_5 - v_{12} - v_{15} - v_{18} - v_{21} + v_{28} + v_{31} \tag{8c}$$

$$\Phi_4^{(5A)} = \Phi_3^{(5)} - \Phi_8^{(5)} = v_3 - v_8 + v_9 - v_{14} - v_{19} + v_{24} - v_{25} + v_{30} \tag{8d}$$

Basis vectors for subspace $S^{(5B)}$

$$\Phi_1^{(5B)} = \Phi_4^{(5)} = v_4 - v_{13} - v_{20} + v_{29} \tag{9a}$$

$$\Phi_2^{(5B)} = \Phi_7^{(5)} = v_7 - v_{10} - v_{23} + v_{26} \tag{9b}$$

$$\Phi_3^{(5B)} = \Phi_2^{(5)} - \Phi_5^{(5)} = v_2 - v_5 + v_{12} - v_{15} - v_{18} + v_{21} - v_{28} + v_{31} \tag{9c}$$

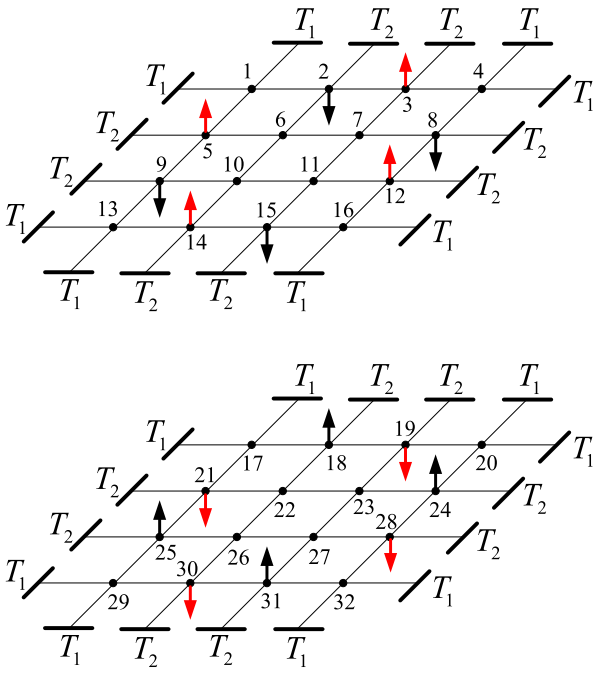

Fig. 5. Unit vertical forces applied in accordance with the coordinates of the basis vector for subspace $S^{(2)}$: Set of unit forces associated with $\Phi_1^{(2)}$. (For interpretation of the references to color in this figure, the reader is referred to the web version of this article.)

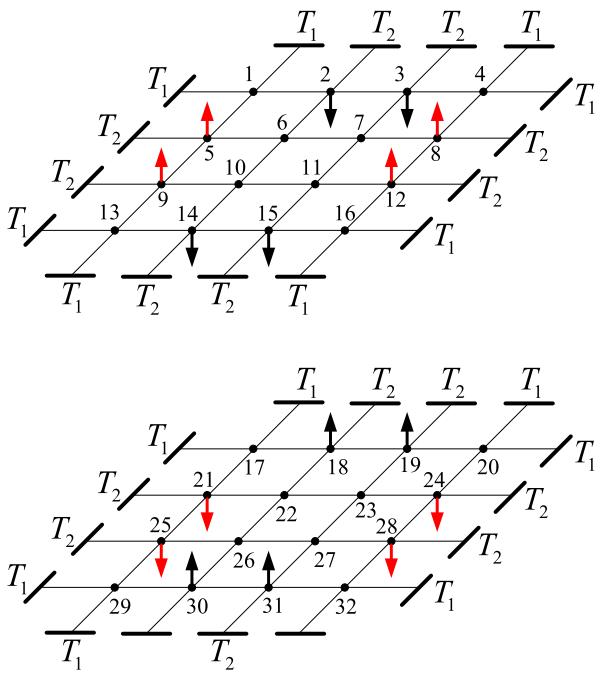

Fig. 6. Unit vertical forces applied in accordance with the coordinates of the basis vector for subspace $S^{(3)}$: Set of unit forces associated with $\Phi_1^{(3)}$. (For interpretation of the references to color in this figure, the reader is referred to the web version of this article.)

$$\Phi_4^{(5B)} = \Phi_3^{(5)} + \Phi_8^{(5)} = v_3 + v_8 - v_9 - v_{14} - v_{19} - v_{24} + v_{25} + v_{30} \tag{9d}$$

Basis vectors for subspace $S^{(6)}$

$$\Phi_1^{(6)} = v_2 - v_3 - v_5 + v_8 + v_9 - v_{12} - v_{14} + v_{15} - v_{18} + v_{19} + v_{21} - v_{24} - v_{25} + v_{28} + v_{30} - v_{31} \tag{10}$$

Basis vectors for subspace $S^{(7)}$

$$\Phi_1^{(7)} = v_1 + v_4 + v_{13} + v_{16} - v_{17} - v_{20} - v_{29} - v_{32} \tag{11a}$$

$$\Phi_2^{(7)} = v_2 + v_3 + v_5 + v_8 + v_9 + v_{12} + v_{14} + v_{15} - v_{18} - v_{19} - v_{21} - v_{24} - v_{25} - v_{28} - v_{30} - v_{31} \tag{11b}$$

$$\Phi_3^{(7)} = v_6 + v_7 + v_{10} + v_{11} - v_{22} - v_{23} - v_{26} - v_{27} \tag{11c}$$

Basis vectors for subspace $S^{(8)}$

$$\Phi_1^{(8)} = v_1 - v_4 - v_{13} + v_{16} - v_{17} + v_{20} + v_{29} - v_{32} \tag{12a}$$

$$\Phi_2^{(8)} = v_2 - v_3 + v_5 - v_8 - v_9 + v_{12} - v_{14} + v_{15} - v_{18} + v_{19} - v_{21} + v_{24} + v_{25} - v_{28} + v_{30} - v_{31} \tag{12b}$$

$$\Phi_3^{(8)} = v_6 - v_7 - v_{10} + v_{11} - v_{22} + v_{23} + v_{26} - v_{27} \tag{12c}$$

Basis vector for subspace $S^{(9)}$

$$\Phi_1^{(9)} = v_2 + v_3 - v_5 - v_8 - v_9 - v_{12} + v_{14} + v_{15} - v_{18} - v_{19} + v_{21} + v_{24} + v_{25} + v_{28} - v_{30} - v_{31} \tag{13}$$

Basis vectors for subspace $S^{(10A)}$

$$\Phi_1^{(10A)} = \Phi_1^{(10)} = v_1 - v_{16} + v_{17} - v_{32} \tag{14a}$$

$$\Phi_2^{(10A)} = \Phi_6^{(10)} = v_6 - v_{11} + v_{22} - v_{27} \tag{14b}$$

$$\Phi_3^{(10A)} = \Phi_2^{(10)} + \Phi_5^{(10)} = v_2 + v_5 - v_{12} - v_{15} + v_{18} + v_{21} - v_{28} - v_{31} \tag{14c}$$

$$\Phi_4^{(10A)} = \Phi_3^{(10)} - \Phi_8^{(10)} = v_3 - v_8 + v_9 - v_{14} + v_{19} - v_{24} + v_{25} - v_{30} \tag{14d}$$

Basis vectors for subspace $S^{(10B)}$

$$\Phi_1^{(10B)} = \Phi_4^{(10)} = v_4 - v_{13} + v_{20} - v_{29} \tag{15a}$$

$$\Phi_2^{(10B)} = \Phi_7^{(10)} = v_7 - v_{10} + v_{23} - v_{26} \tag{15b}$$

$$\Phi_3^{(10B)} = \Phi_2^{(10)} - \Phi_5^{(10)} = v_2 - v_5 + v_{12} - v_{15} + v_{18} - v_{21} + v_{28} - v_{31} \tag{15c}$$

$$\Phi_4^{(10B)} = \Phi_3^{(10)} + \Phi_8^{(10)} = v_3 + v_8 - v_9 - v_{14} + v_{19} + v_{24} - v_{25} - v_{30} \tag{15d}$$

5. Symmetry-adapted flexibility matrices

Figs. 4 to 13 show, for subspace $S^{(1)}$ up to $S^{(10)}$, unit vertical forces applied upon the cable-net nodes in accordance with the coordinates of the respective basis vectors. As explained previously (Zingoni, 2018), consideration of either subspace $S^{(5A)}$ or $S^{(5B)}$ will yield all the 8 natural frequencies of subspace $S^{(5)}$, which occur as four sets of repeated roots. Similarly, consideration of either subspace $S^{(10A)}$ or $S^{(10B)}$ will yield all the 8 natural frequencies of subspace $S^{(10)}$, which also occur as four sets of repeated roots. We

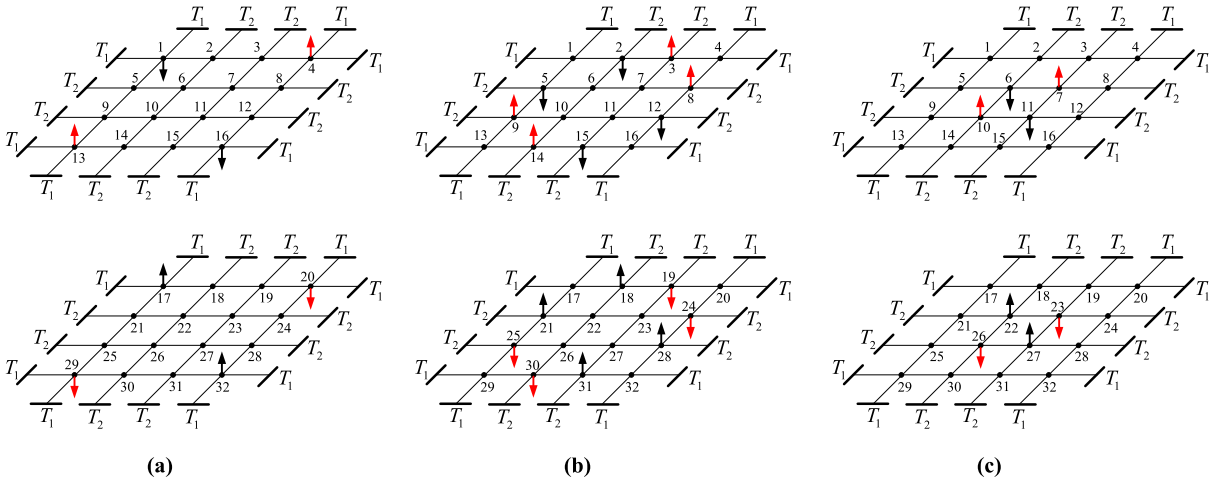

Fig. 7. Unit vertical forces applied in accordance with the coordinates of the basis vectors for subspace $S^{(4)}$: (a) Set of unit forces associated with $\Phi_1^{(4)}$; (b) Set of unit forces associated with $\Phi_2^{(4)}$; (c) Set of unit forces associated with $\Phi_3^{(4)}$. (For interpretation of the references to color in this figure, the reader is referred to the web version of this article.)

have chosen subspaces $S^{(5A)}$ and $S^{(10A)}$ as representative of subspaces $S^{(5)}$ and $S^{(10)}$.

In plotting the set of unit vertical forces for each basis vector, the top and bottom layers of the cable net are shown separately (one below the other), for clarity. The sign (positive or negative) of the unit vertical force applied at a given node is given by the sign of the corresponding basis-vector component. Consistent with our convention for displacements, the positive direction of the unit vertical forces is taken as the direction towards the central horizontal plane of symmetry of the double-layer cable net (i.e. downward for top-layer nodes, and upward for bottom-layer nodes). To enhance clarity, positive unit forces are shown in black, while negative unit forces are shown in red. As an example, the basis vector $\Phi_1^{(1)}$ of subspace $S^{(1)}$ – refer to Eq. (4a) – has eight components $\{v_1, v_4, v_{13}, v_{16}, v_{17}, v_{20}, v_{29}, v_{32}\}$, which are all positive. So in plotting Fig. 4(a), unit vertical forces are shown pointing downwards at the top-layer nodes 1, 4, 13 and 16, and pointing upwards at the bottom-layer nodes 17, 20, 29 and 32, all being in black.

For a given subspace spanned by r basis vectors, let d_{ij} ($i = 1, 2, \ldots, r$; $j = 1, 2, \ldots, r$) be the vertical displacement at *any* of the nodes of the basis vector Φ_i, due to unit vertical forces simultaneously applied at *all* the nodes of the basis vector Φ_j. At each node of the cable net experiencing the vertical displacement d_{ij}, the vertical resultants of the cable tensions will be in equilibrium with the spring force, and any unit vertical force that may be acting at that node. Setting $a = b$ (equal cable spacing in both the x and y directions), and using the values of cable forces and spring stiffnesses applicable for the node in question (refer to Figs 2 and 3), we can make use of either of Eqs. (1) to write down the equilibrium equation for the node. As a result of applying unit vertical forces at *all* the nodes of the basis vector Φ_j, the condition of vertical equilibrium at each of the r sets of nodes (corresponding to the r basis vectors of the subspace) leads to r simultaneous equations in the r deflection unknowns $\{d_{1j}, d_{2j}, \ldots, d_{rj}\}$, which may be expressed as follows:

$$\begin{bmatrix} b_{11} & b_{12} & . & b_{1r} \\ b_{21} & b_{22} & . & b_{2r} \\ . & . & . & . \\ b_{r1} & b_{r2} & . & b_{rr} \end{bmatrix} \begin{Bmatrix} d_{1j} \\ d_{2j} \\ . \\ d_{rj} \end{Bmatrix} = \begin{Bmatrix} \delta_{1j} \\ \delta_{2j} \\ . \\ \delta_{rj} \end{Bmatrix} \tag{16}$$

for $j = 1, 2, \ldots, r$; $\delta_{ij} = 1$ if $i = j$, $\delta_{ij} = 0$ if $i \neq j$. This equation can be written as

$$\left[B^{(\mu)}\right]\{d_j\} = \{\delta_j\} \tag{17}$$

where $[B^{(\mu)}]$ is the $r \times r$ equilibrium matrix corresponding to subspace $S^{(\mu)}$; $\{\delta_j\}$ is an $r \times 1$ column vector consisting of a "1" at row j and "zeros" everywhere else; and $\{d_j\}$ is the $r \times 1$ column vector of deflections corresponding to the application of unit vertical forces at each of the nodes of Φ_j. Thus the elements of $\{d_j\}$ are the flexibility coefficients corresponding to the application of unit vertical forces at the nodes of Φ_j.

Re-arranging Eq. (17), we obtain the solution for the $\{d_j\}$ as follows:

$$\{d_j\} = \left[B^{(\mu)}\right]^{-1}\{\delta_j\}; \quad j = 1, 2, \ldots, r \tag{18}$$

where the column vectors $\{\delta_j\}$ are as defined above. Putting together the solutions for the column vectors $\{d_j\}$ for all values of j (i.e. $j = 1, 2, \ldots, r$), we obtain the assembled $r \times r$ flexibility matrix for subspace $S^{(\mu)}$, which we will denote by $[A^{(\mu)}]$, as follows:

$$\left[A^{(\mu)}\right] = \left[\{d_1\} \quad \{d_2\} \quad . \quad . \quad . \quad \{d_r\}\right] \tag{19}$$

Below, we derive the $[B^{(\mu)}]$ matrix for each of the ten subspaces of the double-layer cable net. We first express, on the basis of Eqs. (1), the conditions of vertical equilibrium at the nodes of each basis vector of the subspace, and then collect these into the form $[B^{(\mu)}]\{d_j\} = [\delta_j]$. This procedure for generating the $[B^{(\mu)}]$ matrices is key to the group-theoretic computational scheme. With the $[B^{(\mu)}]$ matrices known, the $\{d_j\}$ may then be evaluated from Eq. (18), and put together in accordance with Eq. (19) to yield, for each subspace $S^{(\mu)}$, the associated symmetry-adapted flexibility matrix $[A^{(\mu)}]$.

Subspace $S^{(1)}$

Simultaneous application of unit vertical forces at all the nodes of the basis vector Φ_j ($j = 1, 2, 3$) – refer to Fig. 4 – yields the following equilibrium equations:

$$\text{At nodes of } \Phi_1: \quad \frac{T_1}{a}\left(2d_{1j} - 0 - d_{2j}\right) + \frac{T_1}{a}\left(2d_{1j} - 0 - d_{2j}\right) + k_1\left(d_{1j} + d_{1j}\right) = \delta_{1j} \tag{20a}$$

$$\text{At nodes of } \Phi_2: \quad \frac{T_1}{a}\left(2d_{2j} - d_{1j} - d_{2j}\right) + \frac{T_2}{a}\left(2d_{2j} - 0 - d_{3j}\right) + k_2\left(d_{2j} + d_{2j}\right) = \delta_{2j} \tag{20b}$$

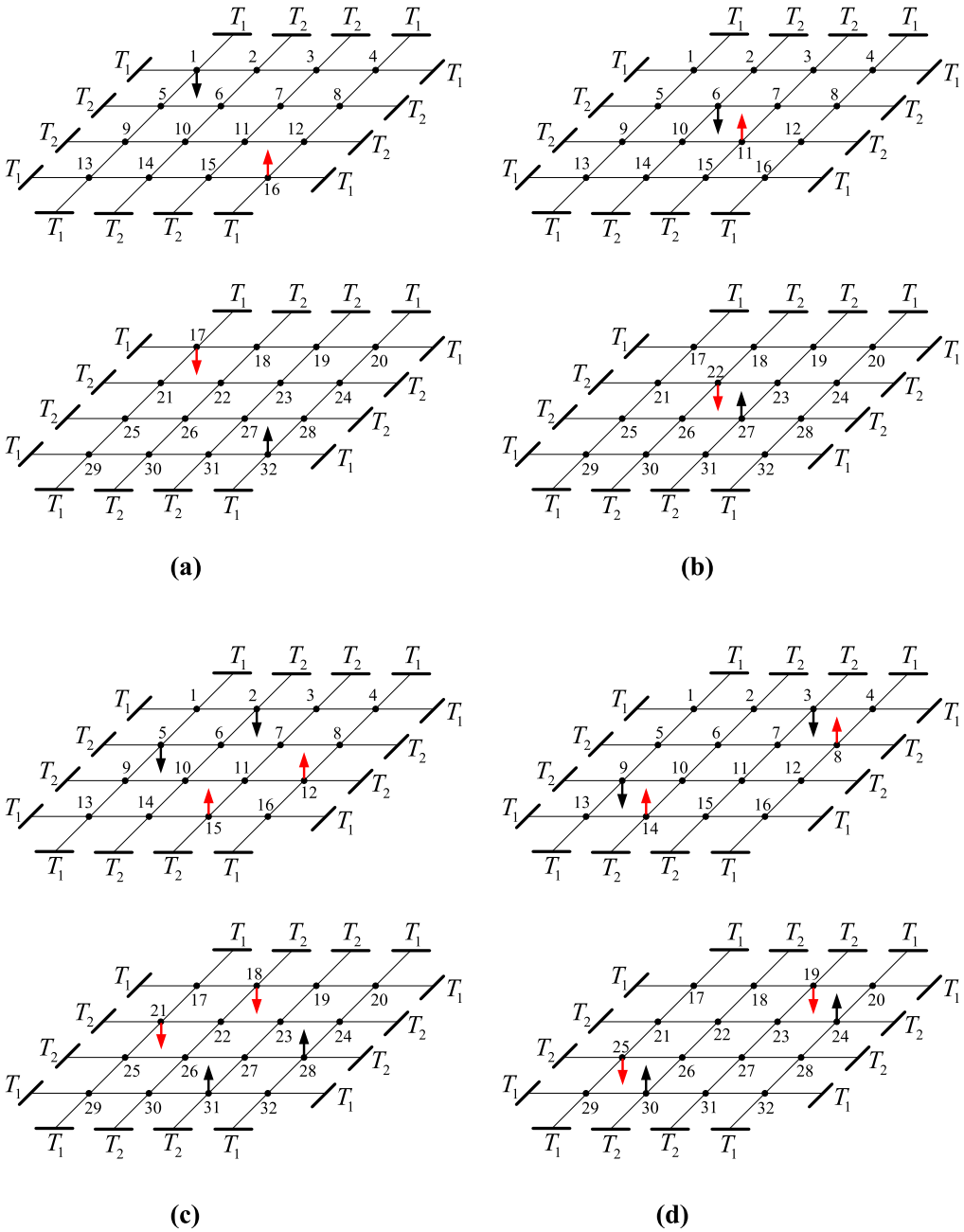

Fig. 8. Unit vertical forces applied in accordance with the coordinates of the basis vectors for subspace $S^{(5A)}$: (a) Set of unit forces associated with $\Phi_1^{(5A)}$; (b) Set of unit forces associated with $\Phi_2^{(5A)}$; (c) Set of unit forces associated with $\Phi_3^{(5A)}$; (d) Set of unit forces associated with $\Phi_4^{(5A)}$. (For interpretation of the references to color in this figure, the reader is referred to the web version of this article.)

$$\textit{At nodes of } \Phi_3: \quad \frac{T_2}{a}\left(2d_{3j}-d_{2j}-d_{3j}\right)+\frac{T_2}{a}\left(2d_{3j}-d_{2j}-d_{3j}\right) + k_3\left(d_{3j}+d_{3j}\right)=\delta_{3j} \tag{20c}$$

Writing these equations in matrix form (i.e. in the format of Eq. (16)), we obtain

$$\begin{bmatrix} \left(\frac{4T_1}{a}+2k_1\right) & -\frac{2T_1}{a} & 0 \\ -\frac{T_1}{a} & \left(\frac{T_1+2T_2}{a}+2k_2\right) & -\frac{T_2}{a} \\ 0 & -\frac{2T_2}{a} & \left(\frac{2T_2}{a}+2k_3\right) \end{bmatrix} \begin{Bmatrix} d_{1j} \\ d_{2j} \\ d_{3j} \end{Bmatrix} = \begin{Bmatrix} \delta_{1j} \\ \delta_{2j} \\ \delta_{3j} \end{Bmatrix} \tag{21}$$

where $\delta_{ij}=1$ if $i=j$; $\delta_{ij}=0$ if $i \neq j$. The required equilibrium matrix for subspace $S^{(1)}$, that is $[B^{(1)}]$, is the 3×3 matrix in the above equation.

Subspace $S^{(2)}$

Simultaneous application of unit vertical forces at all the nodes of the basis vector Φ_j $(j=1)$ – refer to Fig. 5 – yields the following equilibrium equation:

$$\textit{At nodes of } \Phi_1: \quad \frac{T_1}{a}\left(2d_{1j}-0+d_{1j}\right)+\frac{T_2}{a}\left(2d_{1j}-0-0\right) + k_2\left(d_{1j}+d_{1j}\right)=\delta_{1j} \tag{22}$$

Writing this equation in matrix form (i.e. in the format of Eq. (16)), we obtain

$$\left[\frac{3T_1+2T_2}{a}+2k_2\right]\left\{d_{1j}\right\}=\left\{\delta_{1j}\right\} \tag{23}$$

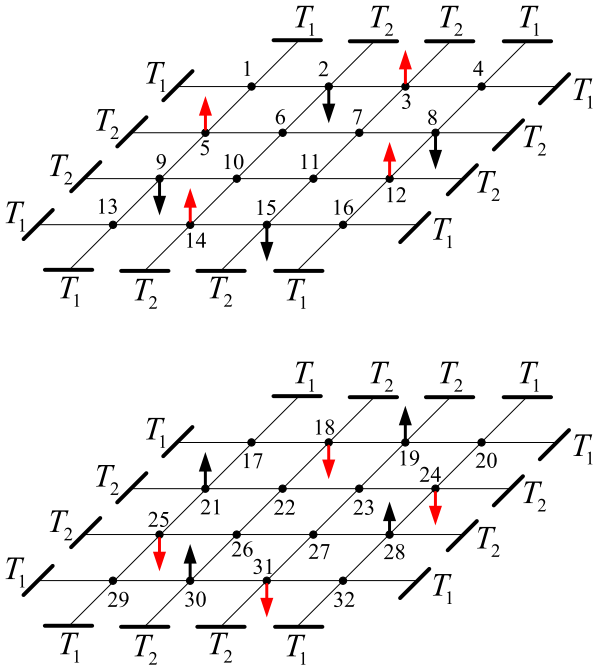

Fig. 9. Unit vertical forces applied in accordance with the coordinates of the basis vector for subspace $S^{(6)}$: Set of unit forces associated with $\Phi_1^{(6)}$. (For interpretation of the references to color in this figure, the reader is referred to the web version of this article.)

where, in this case, $\{d_{1j}\}=\{d_{11}\}$ and $\{\delta_{ij}\}=\{\delta_{11}\}=1$. The equilibrium matrix for subspace $S^{(2)}$, that is $[B^{(2)}]$, is the 1×1 matrix in the above equation. In this very simple case, the subspace flexibility matrix $[A^{(2)}]$ is a 1×1 matrix, and immediately follows from Eqs. (19) and (23):

$$\left[A^{(2)}\right]=[\{d_1\}]=[d_{11}]=\left[\frac{1}{\frac{3T_1+2T_2}{a}+2k_2}\right] \tag{24}$$

Subspace $S^{(3)}$

Simultaneous application of unit vertical forces at all the nodes of the basis vector Φ_j $(j=1)$ – refer to Fig. 6 – yields the following equilibrium equation:

$$\begin{aligned}&\text{At nodes of } \Phi_1: \quad \frac{T_1}{a}\left(2d_{1j}-0-d_{1j}\right)+\frac{T_2}{a}\left(2d_{1j}-0-0\right)\\&+k_2\left(d_{1j}+d_{1j}\right)=\delta_{1j}\end{aligned} \tag{25}$$

Writing this equation in matrix form (i.e. in the format of Eq. (16)), we obtain

$$\left[\frac{T_1+2T_2}{a}+2k_2\right]\left\{d_{1j}\right\}=\left\{\delta_{1j}\right\} \tag{26}$$

where, in this case, $\{d_{1j}\}=\{d_{11}\}$ and $\{\delta_{ij}\}=\{\delta_{11}\}=1$. The equilibrium matrix for subspace $S^{(3)}$, that is $[B^{(3)}]$, is the 1×1 matrix in the above equation. In this very simple case, the subspace flexibility matrix $[A^{(3)}]$ is a 1×1 matrix, and immediately follows from Eqs. (19) and (26):

$$\left[A^{(3)}\right]=[\{d_1\}]=[d_{11}]=\left[\frac{1}{\frac{T_1+2T_2}{a}+2k_2}\right] \tag{27}$$

Subspace $S^{(4)}$

Simultaneous application of unit vertical forces at all the nodes of the basis vector Φ_j $(j=1,\ 2,\ 3)$ – refer to Fig. 7 – yields the following equilibrium equations:

$$\begin{aligned}&\text{At nodes of } \Phi_1: \quad \frac{T_1}{a}\left(2d_{1j}-0-d_{2j}\right)+\frac{T_1}{a}\left(2d_{1j}-0-d_{2j}\right)\\&+k_1\left(d_{1j}+d_{1j}\right)=\delta_{1j}\end{aligned} \tag{28a}$$

$$\begin{aligned}&\text{At nodes of } \Phi_2: \quad \frac{T_1}{a}\left(2d_{2j}-d_{1j}+d_{2j}\right)+\frac{T_2}{a}\left(2d_{2j}-0-d_{3j}\right)\\&+k_2\left(d_{2j}+d_{2j}\right)=\delta_{2j}\end{aligned} \tag{28b}$$

$$\begin{aligned}&\text{At nodes of } \Phi_3: \quad \frac{T_2}{a}\left(2d_{3j}-d_{2j}+d_{3j}\right)+\frac{T_2}{a}\left(2d_{3j}-d_{2j}+d_{3j}\right)\\&+k_3\left(d_{3j}+d_{3j}\right)=\delta_{3j}\end{aligned} \tag{28c}$$

Writing these equations in matrix form (i.e. in the format of Eq. (16)), we obtain

$$\begin{bmatrix}\left(\frac{4T_1}{a}+2k_1\right) & -\frac{2T_1}{a} & 0\\ -\frac{T_1}{a} & \left(\frac{3T_1+2T_2}{a}+2k_2\right) & -\frac{T_2}{a}\\ 0 & -\frac{2T_2}{a} & \left(\frac{6T_2}{a}+2k_3\right)\end{bmatrix}\begin{Bmatrix}d_{1j}\\ d_{2j}\\ d_{3j}\end{Bmatrix}=\begin{Bmatrix}\delta_{1j}\\ \delta_{2j}\\ \delta_{3j}\end{Bmatrix} \tag{29}$$

where $\delta_{ij}=1$ if $i=j$; $\delta_{ij}=0$ if $i\neq j$. The required equilibrium matrix for subspace $S^{(4)}$, that is $[B^{(4)}]$, is the 3×3 matrix in the above equation.

Subspace $S^{(5A)}$

Simultaneous application of unit vertical forces at all the nodes of the basis vector Φ_j $(j=1,\ 2,\ 3,\ 4)$ – refer to Fig. 8 – yields the following equilibrium equations:

$$\begin{aligned}&\text{At nodes of } \Phi_1: \quad \frac{T_1}{a}\left(2d_{1j}-0-d_{3j}\right)+\frac{T_1}{a}\left(2d_{1j}-0-d_{3j}\right)\\&+k_1\left(d_{1j}-d_{1j}\right)=\delta_{1j}\end{aligned} \tag{30a}$$

$$\begin{aligned}&\text{At nodes of } \Phi_2: \quad \frac{T_2}{a}\left(2d_{2j}-d_{3j}-0\right)+\frac{T_2}{a}\left(2d_{2j}-d_{3j}-0\right)\\&+k_3\left(d_{2j}-d_{2j}\right)=\delta_{2j}\end{aligned} \tag{30b}$$

$$\begin{aligned}&\text{At nodes of } \Phi_3: \quad \frac{T_1}{a}\left(2d_{3j}-d_{1j}-d_{4j}\right)+\frac{T_2}{a}\left(2d_{3j}-0-d_{2j}\right)\\&+k_2\left(d_{3j}-d_{3j}\right)=\delta_{3j}\end{aligned} \tag{30c}$$

$$\begin{aligned}&\text{At nodes of } \Phi_4: \quad \frac{T_1}{a}\left(2d_{4j}-d_{3j}-0\right)+\frac{T_2}{a}\left(2d_{4j}-0-0\right)\\&+k_2\left(d_{4j}-d_{4j}\right)=\delta_{4j}\end{aligned} \tag{30d}$$

Writing these equations in matrix form (i.e. in the format of Eq. (16)), we obtain

$$\begin{bmatrix}\frac{4T_1}{a} & 0 & -\frac{2T_1}{a} & 0\\ 0 & \frac{4T_2}{a} & -\frac{2T_2}{a} & 0\\ -\frac{T_1}{a} & -\frac{T_2}{a} & \frac{2(T_1+T_2)}{a} & -\frac{T_1}{a}\\ 0 & 0 & -\frac{T_1}{a} & \frac{2(T_1+T_2)}{a}\end{bmatrix}\begin{Bmatrix}d_{1j}\\ d_{2j}\\ d_{3j}\\ d_{4j}\end{Bmatrix}=\begin{Bmatrix}\delta_{1j}\\ \delta_{2j}\\ \delta_{3j}\\ \delta_{4j}\end{Bmatrix} \tag{31}$$

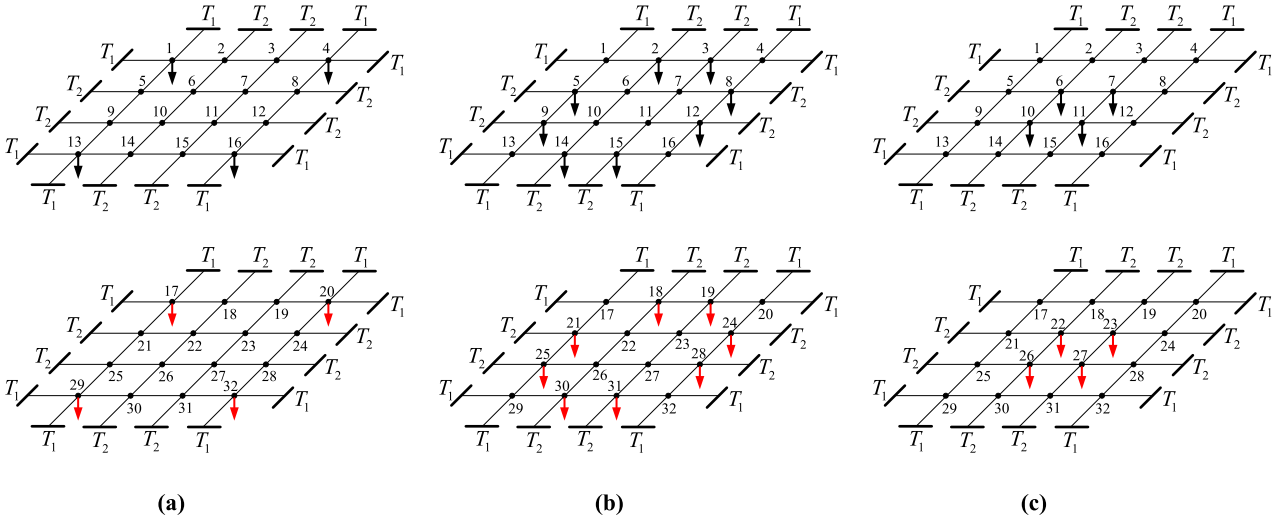

Fig. 10. Unit vertical forces applied in accordance with the coordinates of the basis vectors for subspace $S^{(7)}$: (a) Set of unit forces associated with $\Phi_1^{(7)}$; (b) Set of unit forces associated with $\Phi_2^{(7)}$; (c) Set of unit forces associated with $\Phi_3^{(7)}$. (For interpretation of the references to color in this figure, the reader is referred to the web version of this article.)

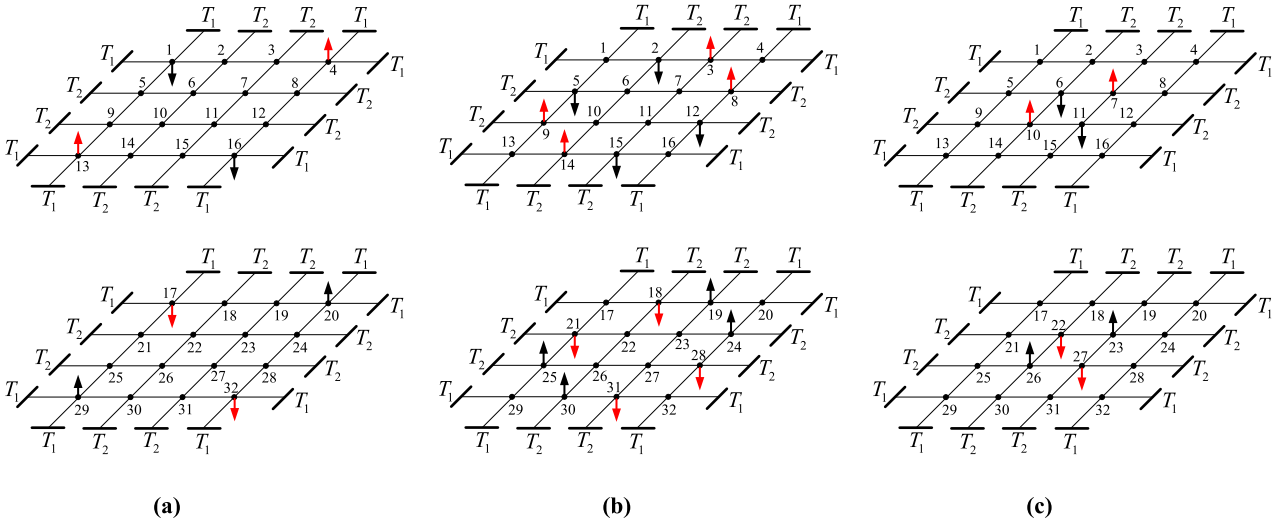

Fig. 11. Unit vertical forces applied in accordance with the coordinates of the basis vectors for subspace $S^{(8)}$: (a) Set of unit forces associated with $\Phi_1^{(8)}$; (b) Set of unit forces associated with $\Phi_2^{(8)}$; (c) Set of unit forces associated with $\Phi_3^{(8)}$. (For interpretation of the references to color in this figure, the reader is referred to the web version of this article.)

where $\delta_{ij}=1$ if $i=j$; $\delta_{ij}=0$ if $i\neq j$. The required equilibrium matrix for subspace $S^{(5A)}$, that is $[B^{(5A)}]$, is the 4×4 matrix in the above equation.

Subspace $S^{(6)}$

Simultaneous application of unit vertical forces at all the nodes of the basis vector Φ_j $(j=1)$ – refer to Fig. 9 – yields the following equilibrium equation:

$$\text{At nodes of } \Phi_1: \quad \frac{T_1}{a}\left(2d_{1j}-0+d_{1j}\right)+\frac{T_2}{a}\left(2d_{1j}-0-0\right) + k_2\left(d_{1j}-d_{1j}\right)=\delta_{1j} \tag{32}$$

Writing this equation in matrix form (i.e. in the format of Eq. (16)), we obtain

$$\left[\frac{3T_1+2T_2}{a}\right]\left\{d_{1j}\right\}=\left\{\delta_{1j}\right\} \tag{33}$$

where, in this case, $\{d_{1j}\}=\{d_{11}\}$ and $\{\delta_{ij}\}=\{\delta_{11}\}=1$. The equilibrium matrix for subspace $S^{(6)}$, that is $[B^{(6)}]$, is the 1×1 matrix in the above equation. In this very simple case, the subspace flexibility matrix $[A^{(6)}]$ is a 1×1 matrix, and immediately follows from Eqs. (19) and (33):

$$\left[A^{(6)}\right]=\left[\{d_1\}\right]=\left[d_{11}\right]=\left[\frac{1}{\frac{3T_1+2T_2}{a}}\right] \tag{34}$$

Subspace $S^{(7)}$

Simultaneous application of unit vertical forces at all the nodes of the basis vector Φ_j $(j=1,\ 2,\ 3)$ – refer to Fig. 10 – yields the following equilibrium equations:

$$\text{At nodes of } \Phi_1: \quad \frac{T_1}{a}\left(2d_{1j}-0-d_{2j}\right)+\frac{T_1}{a}\left(2d_{1j}-0-d_{2j}\right) + k_1\left(d_{1j}-d_{1j}\right)=\delta_{1j} \tag{35a}$$

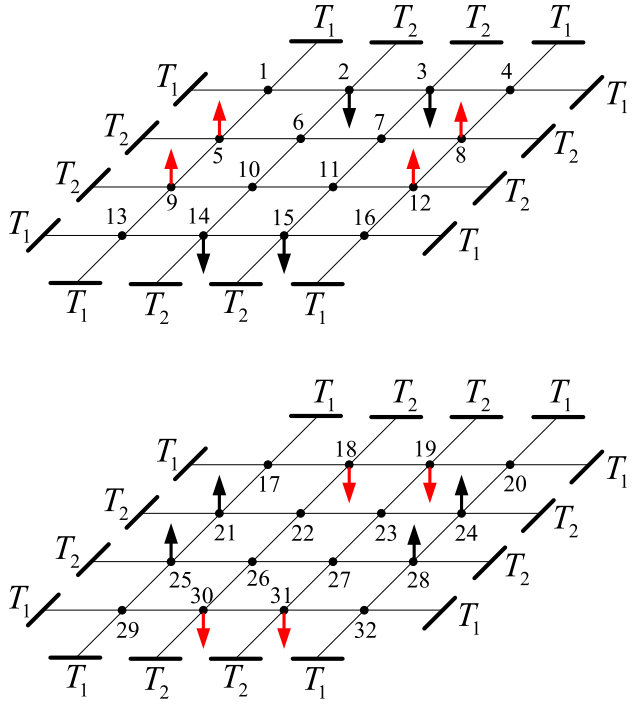

Fig. 12. Unit vertical forces applied in accordance with the coordinates of the basis vector for subspace $S^{(9)}$: Set of unit forces associated with $\Phi_1^{(9)}$. (For interpretation of the references to color in this figure, the reader is referred to the web version of this article.)

$$\textit{At nodes of } \Phi_2: \quad \frac{T_1}{a}\left(2d_{2j}-d_{1j}-d_{2j}\right)+\frac{T_2}{a}\left(2d_{2j}-0-d_{3j}\right) + k_2\left(d_{2j}-d_{2j}\right)=\delta_{2j} \tag{35b}$$

$$\textit{At nodes of } \Phi_3: \quad \frac{T_2}{a}\left(2d_{3j}-d_{2j}-d_{3j}\right)+\frac{T_2}{a}\left(2d_{3j}-d_{2j}-d_{3j}\right) + k_3\left(d_{3j}-d_{3j}\right)=\delta_{3j} \tag{35c}$$

Writing these equations in matrix form (i.e. in the format of Eq. (16)), we obtain

$$\begin{bmatrix} \frac{4T_1}{a} & -\frac{2T_1}{a} & 0 \\ -\frac{T_1}{a} & \frac{T_1+2T_2}{a} & -\frac{T_2}{a} \\ 0 & -\frac{2T_2}{a} & \frac{2T_2}{a} \end{bmatrix} \begin{Bmatrix} d_{1j} \\ d_{2j} \\ d_{3j} \end{Bmatrix} = \begin{Bmatrix} \delta_{1j} \\ \delta_{2j} \\ \delta_{3j} \end{Bmatrix} \tag{36}$$

where $\delta_{ij}=1$ if $i=j$; $\delta_{ij}=0$ if $i \neq j$. The required equilibrium matrix for subspace $S^{(7)}$, that is $[B^{(7)}]$, is the 3×3 matrix in the above equation.

Subspace $S^{(8)}$

Simultaneous application of unit vertical forces at all the nodes of the basis vector Φ_j ($j=1,\ 2,\ 3$) – refer to Fig. 11 – yields the following equilibrium equations:

$$\textit{At nodes of } \Phi_1: \quad \frac{T_1}{a}\left(2d_{1j}-0-d_{2j}\right)+\frac{T_1}{a}\left(2d_{1j}-0-d_{2j}\right) + k_1\left(d_{1j}-d_{1j}\right)=\delta_{1j} \tag{37a}$$

$$\textit{At nodes of } \Phi_2: \quad \frac{T_1}{a}\left(2d_{2j}-d_{1j}+d_{2j}\right)+\frac{T_2}{a}\left(2d_{2j}-0-d_{3j}\right) + k_2\left(d_{2j}-d_{2j}\right)=\delta_{2j} \tag{37b}$$

$$\textit{At nodes of } \Phi_3: \quad \frac{T_2}{a}\left(2d_{3j}-d_{2j}+d_{3j}\right)+\frac{T_2}{a}\left(2d_{3j}-d_{2j}+d_{3j}\right) + k_3\left(d_{3j}-d_{3j}\right)=\delta_{3j} \tag{37c}$$

Writing these equations in matrix form (i.e. in the format of Eq. (16)), we obtain

$$\begin{bmatrix} \frac{4T_1}{a} & -\frac{2T_1}{a} & 0 \\ -\frac{T_1}{a} & \frac{3T_1+2T_2}{a} & -\frac{T_2}{a} \\ 0 & -\frac{2T_2}{a} & \frac{6T_2}{a} \end{bmatrix} \begin{Bmatrix} d_{1j} \\ d_{2j} \\ d_{3j} \end{Bmatrix} = \begin{Bmatrix} \delta_{1j} \\ \delta_{2j} \\ \delta_{3j} \end{Bmatrix} \tag{38}$$

where $\delta_{ij}=1$ if $i=j$; $\delta_{ij}=0$ if $i \neq j$. The required equilibrium matrix for subspace $S^{(8)}$, that is $[B^{(8)}]$, is the 3×3 matrix in the above equation.

Subspace $S^{(9)}$

Simultaneous application of unit vertical forces at all the nodes of the basis vector Φ_j ($j=1$) – refer to Fig. 12 – yields the following equilibrium equation:

$$\textit{At nodes of } \Phi_1: \quad \frac{T_1}{a}\left(2d_{1j}-0-d_{1j}\right)+\frac{T_2}{a}\left(2d_{1j}-0-0\right) + k_2\left(d_{1j}-d_{1j}\right)=\delta_{1j} \tag{39}$$

Writing this equation in matrix form (i.e. in the format of Eq. (16)), we obtain

$$\left[\frac{T_1+2T_2}{a}\right]\left\{d_{1j}\right\}=\left\{\delta_{1j}\right\} \tag{40}$$

where, in this case, $\{d_{1j}\}=\{d_{11}\}$ and $\{\delta_{ij}\}=\{\delta_{11}\}=1$. The equilibrium matrix for subspace $S^{(9)}$, that is $[B^{(9)}]$, is the 1×1 matrix in the above equation. In this very simple case, the subspace flexibility matrix $[A^{(9)}]$ is a 1×1 matrix, and immediately follows from Eqs. (19) and (40):

$$\left[A^{(9)}\right]=\left[\{d_1\}\right]=\left[d_{11}\right]=\left[\frac{1}{\frac{T_1+2T_2}{a}}\right] \tag{41}$$

Subspace $S^{(10A)}$

Simultaneous application of unit vertical forces at all the nodes of the basis vector Φ_j ($j=1,\ 2,\ 3,\ 4$) – refer to Fig. 13 – yields the following equilibrium equations:

$$\textit{At nodes of } \Phi_1: \quad \frac{T_1}{a}\left(2d_{1j}-0-d_{3j}\right)+\frac{T_1}{a}\left(2d_{1j}-0-d_{3j}\right) + k_1\left(d_{1j}+d_{1j}\right)=\delta_{1j} \tag{42a}$$

$$\textit{At nodes of } \Phi_2: \quad \frac{T_2}{a}\left(2d_{2j}-d_{3j}-0\right)+\frac{T_2}{a}\left(2d_{2j}-d_{3j}-0\right) + k_3\left(d_{2j}+d_{2j}\right)=\delta_{2j} \tag{42b}$$

$$\textit{At nodes of } \Phi_3: \quad \frac{T_1}{a}\left(2d_{3j}-d_{1j}-d_{4j}\right)+\frac{T_2}{a}\left(2d_{3j}-0-d_{2j}\right) + k_2\left(d_{3j}+d_{3j}\right)=\delta_{3j} \tag{42c}$$

$$\textit{At nodes of } \Phi_4: \quad \frac{T_1}{a}\left(2d_{4j}-d_{3j}-0\right)+\frac{T_2}{a}\left(2d_{4j}-0-0\right) + k_2\left(d_{4j}+d_{4j}\right)=\delta_{4j} \tag{42d}$$

Writing these equations in matrix form (i.e. in the format of Eq. (16)), we obtain

Table 1
Degrees of characteristic equations of subspaces of the 32-node double-layer cable net.

Subspace	$\kappa\ (=r)$
$S^{(1)}$	3
$S^{(2)}$	1
$S^{(3)}$	1
$S^{(4)}$	3
$S^{(5A)}$	4
$S^{(5B)}$	4
$S^{(6)}$	1
$S^{(7)}$	3
$S^{(8)}$	3
$S^{(9)}$	1
$S^{(10A)}$	4
$S^{(10B)}$	4
Full Space	32

$$\begin{bmatrix} \left(\frac{4T_1}{a}+2k_1\right) & 0 & -\frac{2T_1}{a} & 0 \\ 0 & \left(\frac{4T_2}{a}+2k_3\right) & -\frac{2T_2}{a} & 0 \\ -\frac{T_1}{a} & -\frac{T_2}{a} & \left(\frac{2(T_1+T_2)}{a}+2k_2\right) & -\frac{T_1}{a} \\ 0 & 0 & -\frac{T_1}{a} & \left(\frac{2(T_1+T_2)}{a}+2k_2\right) \end{bmatrix} \begin{Bmatrix} d_{1j} \\ d_{2j} \\ d_{3j} \\ d_{4j} \end{Bmatrix} = \begin{Bmatrix} \delta_{1j} \\ \delta_{2j} \\ \delta_{3j} \\ \delta_{4j} \end{Bmatrix} \tag{43}$$

where $\delta_{ij}=1$ if $i=j$; $\delta_{ij}=0$ if $i\neq j$. The required equilibrium matrix for subspace $S^{(10A)}$, that is $[B^{(10A)}]$, is the 4×4 matrix in the above equation.

6. Subspace mass matrices

As already pointed out in Section 4.1, the distribution of concentrated masses at the nodes of the double-layer cable net is consistent with the overall D_{4h} symmetry of the net. Nodes belonging to the same permutation set under the operation of the elements of group D_{4h} have the same values of mass, designated as follows (see Fig. 3):

- corner nodes {1, 4, 13, 16, 17, 20, 29, 32}: m_1
- mid-side nodes {2, 3, 5, 8, 9, 12, 14, 15, 18, 19, 21, 24, 25, 28, 30, 31}: m_2
- centre nodes {6, 7, 10, 11, 22, 23, 26, 27}: m_3

The symmetry-adapted diagonal mass matrix $[M^{(\mu)}]$ for a given subspace $S^{(\mu)}$ consists of non-zero diagonal elements m_{ii} $(i=1,\ 2,\ \ldots,\ r)$, which are the values of the mass at each of the nodes of basis vector Φ_i. Thus for the ten subspaces of our problem, the results for symmetry-adapted mass matrices are as follows:

$$\left[M^{(1)}\right]=\left[M^{(4)}\right]=\left[M^{(7)}\right]=\left[M^{(8)}\right]=\begin{bmatrix} m_1 & 0 & 0 \\ 0 & m_2 & 0 \\ 0 & 0 & m_3 \end{bmatrix} \tag{44}$$

$$\left[M^{(2)}\right]=\left[M^{(3)}\right]=\left[M^{(6)}\right]=\left[M^{(9)}\right]=[m_2] \tag{45}$$

$$\left[M^{(5A)}\right]=\left[M^{(10A)}\right]=\begin{bmatrix} m_1 & 0 & 0 & 0 \\ 0 & m_3 & 0 & 0 \\ 0 & 0 & m_2 & 0 \\ 0 & 0 & 0 & m_2 \end{bmatrix} \tag{46}$$

7. Eigenvalues and eigenvectors

Eigenvalues $\lambda\ (=1/\omega^2$, where ω is a natural circular frequency of the system) for each subspace are obtained from the vanishing condition of the determinant:

$$\left|\left[A^{(\mu)}\right]-\lambda\left[M^{(\mu)}\right]^{-1}\right|=0 \tag{47}$$

where $[A^{(\mu)}]$, the subspace flexibility matrix, consists of elements d_{ij} $(i=1,\ 2,\ \ldots,\ r;\ j=1,\ 2,\ \ldots,\ r)$ as obtained in Section 5, and $[M^{(\mu)}]$, the subspace mass matrix, consists of non-zero diagonal elements m_{ii} $(i=1,\ 2,\ \ldots,\ r)$ as obtained in Section 6. Written in expanded form, the above determinant becomes

$$\begin{vmatrix} (d_{11}-(\lambda/m_{11})) & d_{12} & . & d_{1r} \\ d_{21} & (d_{22}-(\lambda/m_{22})) & . & d_{2r} \\ . & . & . & . \\ d_{r1} & d_{r2} & . & (d_{rr}-(\lambda/m_{rr})) \end{vmatrix}=0 \tag{48}$$

which may be expanded into an rth-degree polynomial (characteristic equation) in λ, and solved for the r roots that are associated with the subspace in question. For the 32-node double-layer cable net, the degrees κ of the characteristic equations of the various subspaces, which are equal to the dimensions r of the respective subspaces, are summarised in Table 1.

Between them, the ten subspaces of our 32-node double-layer cable net yield a total of 32 eigenvalues (bearing in mind that the solutions for subspaces $S^{(5A)}$ and $S^{(10A)}$ are doubly repeating roots). These are, in fact, the actual eigenvalues of the original problem, which completes the determination of all 32 natural frequencies of vibration of the cable net. For a formal proof that eigenvalues yielded by the various symmetry subspaces are also eigenvalues of the full space of the original problem, reference may be made to any of the well-known classical texts on physical applications of group theory (see, for example, references (Weyl, 1932; Wigner, 1959; Hamermesh, 1962; Schonland, 1965)).

From the above, it can be seen how effectively the group-theoretic procedure has simplified the determination of eigenvalues (natural frequencies) of the cable net. Instead of tackling a 32 d.o.f. system and eventually having to solve a polynomial equation of degree 32, the group-theoretic approach has decomposed the problem into ten subspaces of smaller dimensions (the highest subspace dimension being only 4), which yield ten polynomial equations of smaller degree (the highest degree being only 4). This clearly represents a considerable reduction in computational effort. It is a quantitative benefit that is additional to the qualitative insights that were gained (Zingoni, 2018) prior to the start of the eigenvalue computations.

The eigenvectors $\{\Psi\}$ for each subspace are obtained by substituting the r eigenvalues of the subspace, one at a time, into the subspace eigenvalue equation

$$\left[\left[A^{(\mu)}\right]-\lambda\left[M^{(\mu)}\right]^{-1}\right]\{\Psi\}=\{0\} \tag{49}$$

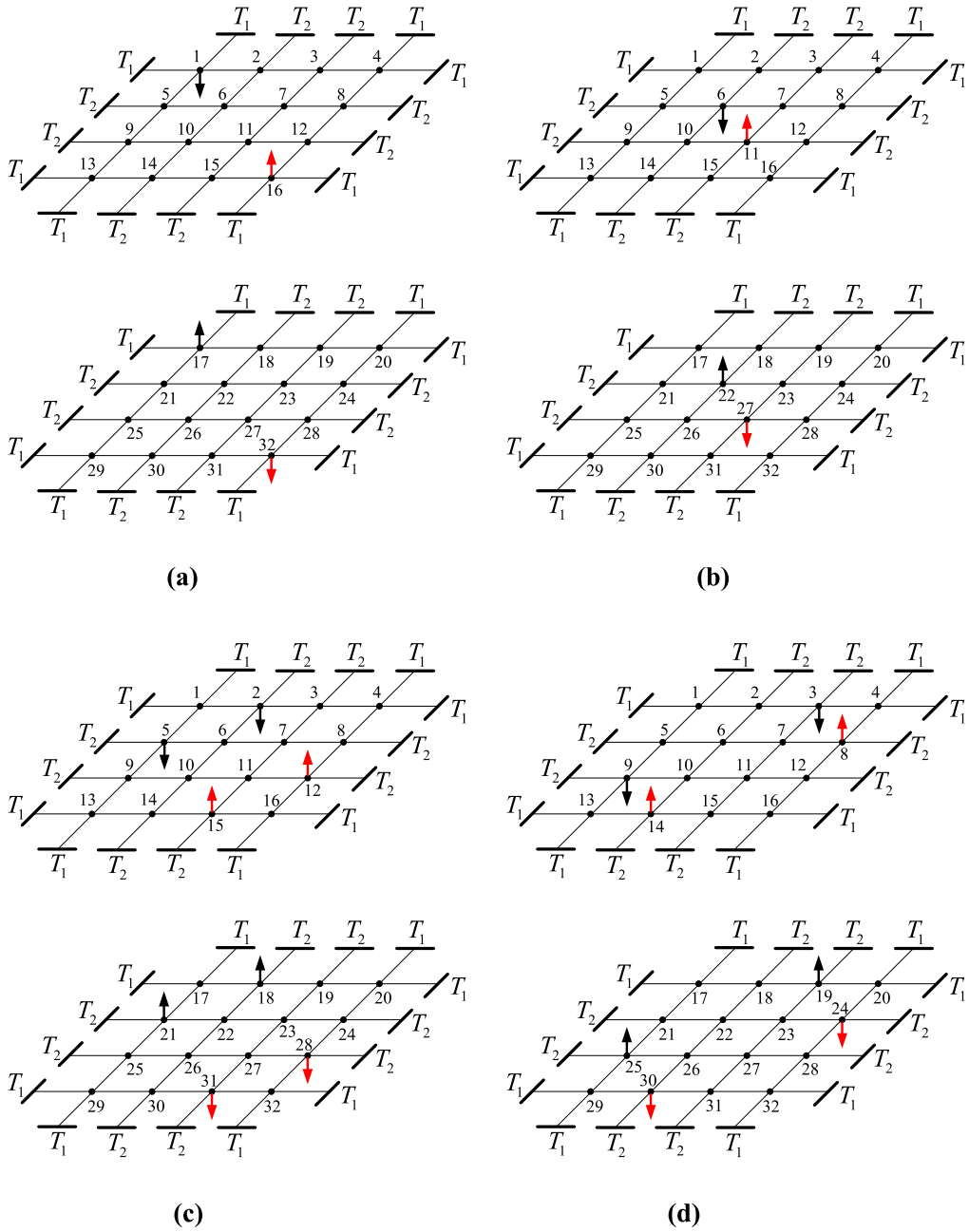

Fig. 13. Unit vertical forces applied in accordance with the coordinates of the basis vectors for subspace $S^{(10A)}$: (a) Set of unit forces associated with $\Phi_1^{(10A)}$; (b) Set of unit forces associated with $\Phi_2^{(10A)}$; (c) Set of unit forces associated with $\Phi_3^{(10A)}$; (d) Set of unit forces associated with $\Phi_4^{(10A)}$. (For interpretation of the references to color in this figure, the reader is referred to the web version of this article.)

Writing this in expanded form, we obtain

$$\begin{bmatrix} (d_{11}-(\lambda/m_{11})) & d_{12} & . & d_{1r} \\ d_{21} & (d_{22}-(\lambda/m_{22})) & . & d_{2r} \\ . & . & . & . \\ d_{r1} & d_{r2} & . & (d_{rr}-(\lambda/m_{rr})) \end{bmatrix} \begin{Bmatrix} \psi_1 \\ \psi_2 \\ . \\ \psi_r \end{Bmatrix} = \begin{Bmatrix} 0 \\ 0 \\ . \\ 0 \end{Bmatrix} \tag{50}$$

So, by substituting a given eigenvalue of the subspace into Eq. (50), and solving for the components $\psi_1, \psi_2, ..., \psi_r$, we obtain the eigenvector $\{\ \psi_1 \quad \psi_2 \quad . \quad \psi_r\ \}^{\mathrm{T}}$ corresponding to that eigenvalue. We repeat the process for all the r eigenvalues of the subspace, in this way generating the r eigenvectors of the subspace. Unlike the r subspace eigenvalues which are also eigenvalues of the original problem, these r eigenvectors are eigenvectors in the r-dimensional subspace, not in the (n-dimensional) full space of the original problem.

We note that the r components $\psi_1, \psi_2, ..., \psi_r$ of a subspace eigenvector correspond to the basis vectors $\Phi_1, \Phi_2, ..., \Phi_r$, respectively, of the subspace in question. Therefore to obtain the *eigenvector* $\{\mathbf{U}\}$ *in the original n-dimensional vector space of the problem*, we simply allocate the calculated value of a subspace-eigenvector component to *all* the cable nodes associated with the basis vector, with the signs (positive or negative) of the allocations being in accordance with those of the basis-vector terms (as appear in Eqs. (4) to (15)).

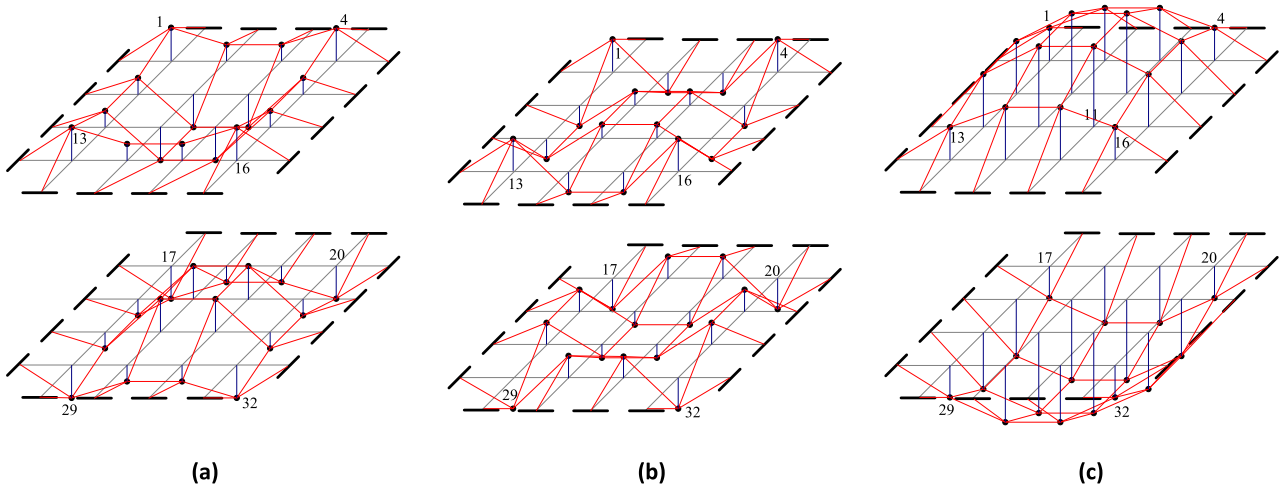

Fig. 14. Vibration modes of subspace $S^{(1)}$ of numerical example: (a) $\mathbf{U}_1^{(1)}$; (b) $\mathbf{U}_2^{(1)}$; (c) $\mathbf{U}_3^{(1)}$. (For interpretation of the references to color in this figure, the reader is referred to the web version of this article.)

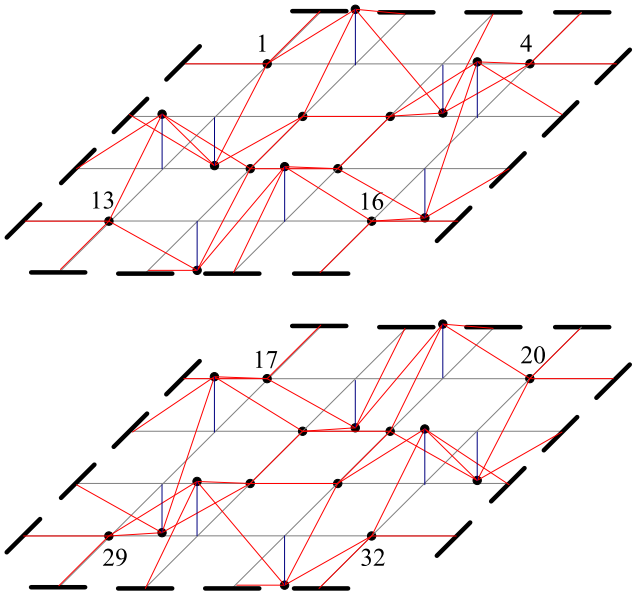

Fig. 15. Vibration mode of subspace $S^{(2)}$ of numerical example: $\mathbf{U}_1^{(2)}$. (For interpretation of the references to color in this figure, the reader is referred to the web version of this article.)

The n deflection components $h_1, h_2, \ldots, h_n$ of the mode shape $\{\mathbf{H}_i\}$ corresponding to the system eigenvector $\{\mathbf{U}_i\}$ are finally obtained through the well-known relationship

$$\{\mathbf{H}_i\} = \left[\mathbf{M}^{-1}\right]\{\mathbf{U}_i\} \tag{51}$$

where $[\mathbf{M}]$ is the conventional diagonal mass matrix of the n degree-of-freedom system. This would then complete the free-vibration analysis of the cable net. To illustrate the full group-theoretic computational procedure, we will consider a numerical example, and present results for natural frequencies and mode shapes.

8. Numerical example

Let us consider a double-layer cable net with the following structural and dynamic parameters:

$T_1 = T_2 = 10$ kN ; $a = 2$ m ; $k_1 = k_2 = k_3 = 10$ kN/m ;

$m_1 = m_2 = m_3 = 10$ kg

First, and using the above parameters, we evaluate the $[B^{(\mu)}]$ matrices of subspaces $S^{(\mu)}$ from Eqs. (21), (23), (26), (29), (31), (33), (36), (38), (40) and (43). Next, the inverses of the $[B^{(\mu)}]$ matrices are evaluated, and used in Eq. (18) to generate the column vectors $\{d_j\}$. The subspace flexibility matrices $[A^{(\mu)}]$ are then assembled by putting together the $\{d_j\}$ column vectors as shown by Eq. (19). The results for the ten subspaces are as follows (with the elements of $[A^{(\mu)}]$ having units of m/kN):

$$\left[A^{(1)}\right] = \begin{bmatrix} \frac{2}{77} & \frac{3}{385} & \frac{1}{770} \\ \frac{3}{770} & \frac{12}{385} & \frac{2}{385} \\ \frac{1}{770} & \frac{4}{385} & \frac{27}{770} \end{bmatrix}\ ;\ \left[A^{(2)}\right] = \left[\frac{1}{45}\right];$$

$$\left[A^{(3)}\right] = \left[\frac{1}{35}\right]\ ;\ \left[A^{(4)}\right] = \begin{bmatrix} \frac{22}{855} & \frac{1}{171} & \frac{1}{1710} \\ \frac{1}{342} & \frac{4}{171} & \frac{2}{855} \\ \frac{1}{1710} & \frac{4}{855} & \frac{7}{342} \end{bmatrix}$$

$$\left[A^{(5A)}\right] = \begin{bmatrix} \frac{13}{220} & \frac{1}{110} & \frac{2}{55} & \frac{1}{110} \\ \frac{1}{110} & \frac{13}{220} & \frac{2}{55} & \frac{1}{110} \\ \frac{1}{55} & \frac{1}{55} & \frac{4}{55} & \frac{1}{55} \\ \frac{1}{220} & \frac{1}{220} & \frac{1}{55} & \frac{3}{55} \end{bmatrix}\ ;\ \left[A^{(6)}\right] = \left[\frac{1}{25}\right];$$

$$\left[A^{(7)}\right] = \begin{bmatrix} \frac{1}{15} & \frac{1}{15} & \frac{1}{30} \\ \frac{1}{30} & \frac{2}{15} & \frac{1}{15} \\ \frac{1}{30} & \frac{2}{15} & \frac{1}{6} \end{bmatrix}$$

$$\left[A^{(8)}\right] = \begin{bmatrix} \frac{7}{125} & \frac{3}{125} & \frac{1}{250} \\ \frac{3}{250} & \frac{6}{125} & \frac{1}{125} \\ \frac{1}{250} & \frac{2}{125} & \frac{9}{250} \end{bmatrix}\ ;\ \left[A^{(9)}\right] = \left[\frac{1}{15}\right];$$

$$\left[A^{(10A)}\right] = \begin{bmatrix} \frac{61}{2360} & \frac{1}{1180} & \frac{2}{295} & \frac{1}{1180} \\ \frac{1}{1180} & \frac{61}{2360} & \frac{2}{295} & \frac{1}{1180} \\ \frac{1}{295} & \frac{1}{295} & \frac{8}{295} & \frac{1}{295} \\ \frac{1}{2360} & \frac{1}{2360} & \frac{1}{295} & \frac{3}{118} \end{bmatrix}$$

Table 2
Deflection ordinates of the three mode shapes of subspace $S^{(1)}$ of the numerical example.

Node	1	2	3	4	5	6	7	8	9	10	11	12	13	14	15	16
$\mathbf{U}_1^{(1)}$	1.00	0.50	0.50	1.00	0.50	−1.00	−1.00	0.50	0.50	−1.00	−1.00	0.50	1.00	0.50	0.50	1.00
$\mathbf{U}_2^{(1)}$	1.00	−0.62	−0.62	1.00	−0.62	0.38	0.38	−0.62	−0.62	0.38	0.38	−0.62	1.00	−0.62	−0.62	1.00
$\mathbf{U}_3^{(1)}$	1.00	1.62	1.62	1.00	1.62	2.62	2.62	1.62	1.62	2.62	2.62	1.62	1.00	1.62	1.62	1.00
Node	17	18	19	20	21	22	23	24	25	26	27	28	29	30	31	32
$\mathbf{U}_1^{(1)}$	1.00	0.50	0.50	1.00	0.50	−1.00	−1.00	0.50	0.50	−1.00	−1.00	0.50	1.00	0.50	0.50	1.00
$\mathbf{U}_2^{(1)}$	1.00	−0.62	−0.62	1.00	−0.62	0.38	0.38	−0.62	−0.62	0.38	0.38	−0.62	1.00	−0.62	−0.62	1.00
$\mathbf{U}_3^{(1)}$	1.00	1.62	1.62	1.00	1.62	2.62	2.62	1.62	1.62	2.62	2.62	1.62	1.00	1.62	1.62	1.00

Table 3
Deflection ordinates of the mode shape of subspace $S^{(2)}$ of the numerical example.

Node	1	2	3	4	5	6	7	8	9	10	11	12	13	14	15	16
$\mathbf{U}_1^{(2)}$	0	+1.00	−1.00	0	−1.00	0	0	+1.00	+1.00	0	0	−1.00	0	−1.00	+1.00	0
Node	17	18	19	20	21	22	23	24	25	26	27	28	29	30	31	32
$\mathbf{U}_1^{(2)}$	0	+1.00	−1.00	0	−1.00	0	0	+1.00	+1.00	0	0	−1.00	0	−1.00	+1.00	0

The subspace mass matrices are written down from Eqs. (44) to (46) as follows (with the elements of $[M^{(\mu)}]$ having units of kg):

$$\left[M^{(1)}\right] = \left[M^{(4)}\right] = \left[M^{(7)}\right] = \left[M^{(8)}\right] = \begin{bmatrix} 10 & 0 & 0 \\ 0 & 10 & 0 \\ 0 & 0 & 10 \end{bmatrix}$$

$$\left[M^{(2)}\right] = \left[M^{(3)}\right] = \left[M^{(6)}\right] = \left[M^{(9)}\right] = [10]$$

$$\left[M^{(5A)}\right] = \left[M^{(10A)}\right] = \begin{bmatrix} 10 & 0 & 0 & 0 \\ 0 & 10 & 0 & 0 \\ 0 & 0 & 10 & 0 \\ 0 & 0 & 0 & 10 \end{bmatrix}$$

The eigenvalues λ of each subspace are obtained by solving Eq. (48), which yields r roots of the characteristic equation, where r is the dimension of the subspace. Now $\lambda = 1/\omega^2$, and the natural frequency of vibration f (cycles per second) is related to the circular frequency ω (radians per second) through the usual relationship $\omega = 2\pi f$. Therefore, $f = 1/(2\pi\sqrt{\lambda})$. For each subspace, the eigenvector Ψ_i corresponding to the eigenvalue λ_i is obtained by solving Eq. (50). For our numerical example, results for subspace eigenvalues λ_i ($i = 1, 2, \ldots, r$), natural frequencies f_i and eigenvectors Ψ_i are as follows:

Subspace $S^{(1)}$

$\lambda_1 = 0.2857$ $\quad f_1 = 0.298$ Hz $\quad \Psi_1 = \begin{bmatrix} 1.000 \\ 0.500 \\ -1.000 \end{bmatrix}$

$\lambda_2 = 0.2165$ $\quad f_2 = 0.342$ Hz $\quad \Psi_2 = \begin{bmatrix} 1.000 \\ -0.618 \\ 0.382 \end{bmatrix}$

$\lambda_3 = 0.4198$ $\quad f_3 = 0.246$ Hz $\quad \Psi_3 = \begin{bmatrix} 1.000 \\ 1.618 \\ 2.618 \end{bmatrix}$

Subspace $S^{(2)}$

$\lambda_1 = 0.2222 \quad f_1 = 0.338$ Hz $\quad \Psi_1 = 1.000$

Subspace $S^{(3)}$

$\lambda_1 = 0.2857 \quad f_1 = 0.298$ Hz $\quad \Psi_1 = 1.000$

Subspace $S^{(4)}$

$\lambda_1 = 0.2222$ $\quad f_1 = 0.338$ Hz $\quad \Psi_1 = \begin{bmatrix} 1.000 \\ -0.500 \\ -1.000 \end{bmatrix}$

$\lambda_2 = 0.1780$ $\quad f_2 = 0.377$ Hz $\quad \Psi_2 = \begin{bmatrix} 1.000 \\ -1.618 \\ 2.618 \end{bmatrix}$

$\lambda_3 = 0.2957$ $\quad f_3 = 0.293$ Hz $\quad \Psi_3 = \begin{bmatrix} 1.000 \\ 0.618 \\ 0.382 \end{bmatrix}$

Subspace $S^{(5A)}$ and $S^{(5B)}$ (these have identical solutions)

$\lambda_1 = 1.1338$ $\quad f_1 = 0.149$ Hz $\quad \Psi_1 = \begin{bmatrix} 1.000 \\ 1.000 \\ 1.118 \\ 0.500 \end{bmatrix}$

$\lambda_2 = 0.5000$ $\quad f_2 = 0.225$ Hz $\quad \Psi_2 = \begin{bmatrix} 1.000 \\ 0 \\ 0 \\ -1.000 \end{bmatrix}$

$\lambda_3 = 0.5000$ $\quad f_3 = 0.225$ Hz $\quad \Psi_3 = \begin{bmatrix} 1.000 \\ -1.000 \\ 0 \\ 0 \end{bmatrix}$

$\lambda_4 = 0.3207$ $\quad f_4 = 0.281$ Hz $\quad \Psi_4 = \begin{bmatrix} 1.000 \\ 1.000 \\ -1.118 \\ 0.500 \end{bmatrix}$

Subspace $S^{(6)}$

$\lambda_1 = 0.4000 \quad f_1 = 0.252$ Hz $\quad \Psi_1 = 1.000$

Subspace $S^{(7)}$

$\lambda_1 = 0.6667$ $\quad f_1 = 0.195$ Hz $\quad \Psi_1 = \begin{bmatrix} 1.000 \\ 0.500 \\ -1.000 \end{bmatrix}$

$\lambda_2 = 0.3820$ $\quad f_2 = 0.258$ Hz $\quad \Psi_2 = \begin{bmatrix} 1.000 \\ -0.618 \\ 0.382 \end{bmatrix}$

$\lambda_3 = 2.6180$ $\quad f_3 = 0.0984$ Hz $\quad \Psi_3 = \begin{bmatrix} 1.000 \\ 1.618 \\ 2.618 \end{bmatrix}$

Subspace $S^{(8)}$

$\lambda_1 = 0.4000$ $\quad f_1 = 0.252$ Hz $\quad \Psi_1 = \begin{bmatrix} 1.000 \\ -0.500 \\ -1.000 \end{bmatrix}$

$\lambda_2 = 0.2764$ $\quad f_2 = 0.303$ Hz $\quad \Psi_2 = \begin{bmatrix} 1.000 \\ -1.618 \\ 2.618 \end{bmatrix}$

$\lambda_3 = 0.7236$ $\quad f_3 = 0.187$ Hz $\quad \Psi_3 = \begin{bmatrix} 1.000 \\ 0.618 \\ 0.382 \end{bmatrix}$

Subspace $S^{(9)}$

$\lambda_1 = 0.6667 \quad f_1 = 0.195$ Hz $\quad \Psi_1 = 1.000$

Subspace $S^{(10A)}$ and $S^{(10B)}$ (these have identical solutions)

$\lambda_1 = 0.3470$ $\quad f_1 = 0.270$ Hz $\quad \Psi_1 = \begin{bmatrix} 1.000 \\ 1.000 \\ 1.118 \\ 0.500 \end{bmatrix}$

$\lambda_2 = 0.2500$ $\quad f_2 = 0.318$ Hz $\quad \Psi_2 = \begin{bmatrix} 1.000 \\ 0 \\ 0 \\ -1.000 \end{bmatrix}$

$\lambda_3 = 0.2500$ $\quad f_3 = 0.318$ Hz $\quad \Psi_3 = \begin{bmatrix} 1.000 \\ -1.000 \\ 0 \\ 0 \end{bmatrix}$

$\lambda_4 = 0.1954$ $\quad f_4 = 0.360$ Hz $\quad \Psi_4 = \begin{bmatrix} 1.000 \\ 1.000 \\ -1.118 \\ 0.500 \end{bmatrix}$

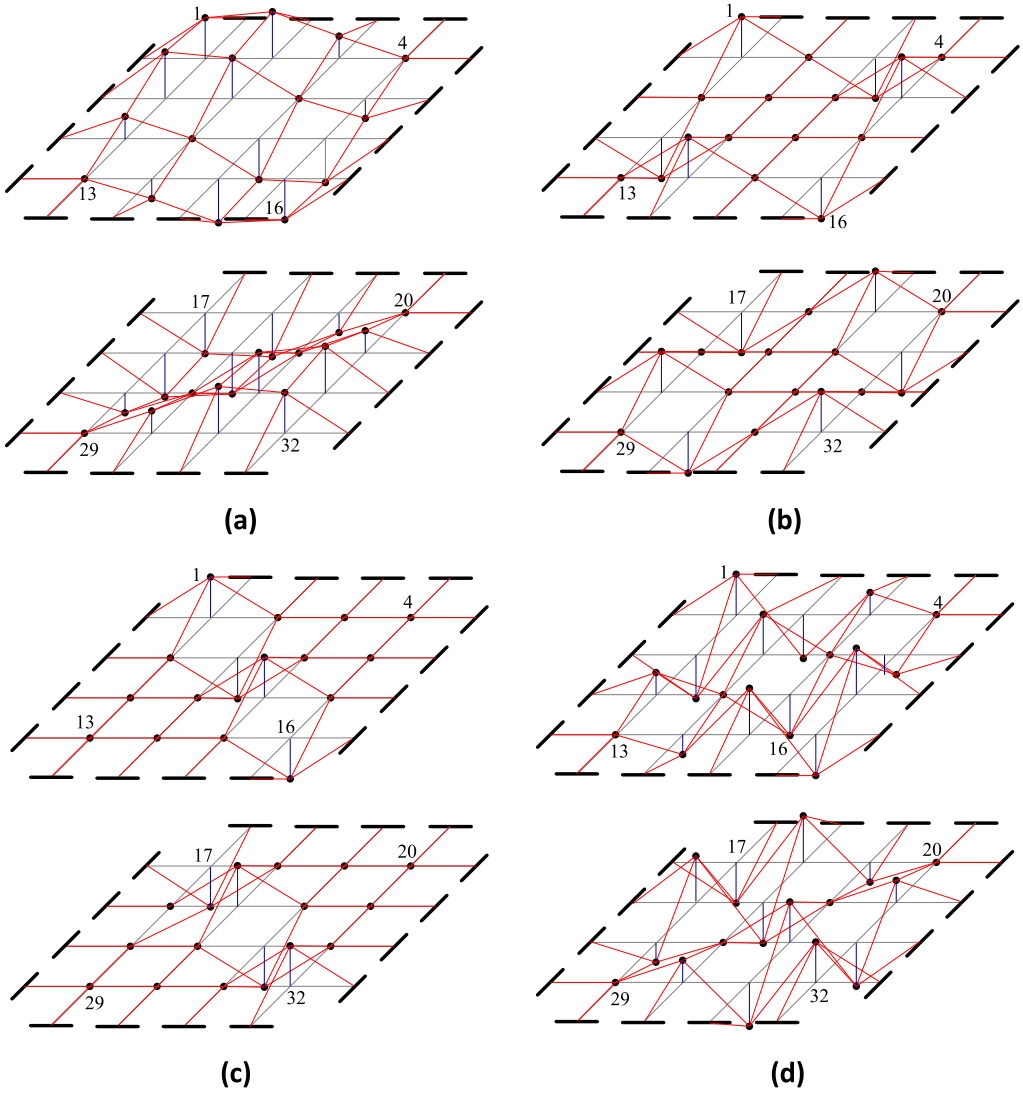

Fig. 16. Vibration modes of subspace $S^{(10A)}$ of numerical example: (a) $\mathbf{U}_1^{(10A)}$; (b) $\mathbf{U}_2^{(10A)}$; (c) $\mathbf{U}_3^{(10A)}$; (d) $\mathbf{U}_4^{(10A)}$. (For interpretation of the references to color in this figure, the reader is referred to the web version of this article.)

To illustrate how mode shapes in the full space of the problem are generated, let us consider subspaces $S^{(1)}$, $S^{(2)}$and $S^{(10A)}$, which are representative of 3-dimensional, 1-dimensional and 4-dimensional subspaces, and which also belong to the extensional vibration modes whose natural frequencies depend on the spring stiffness parameter k. As explained in Section 7, eigenvectors $\{\mathbf{U}_i\}$ in the 32-dimensional vector space of the original problem are obtained by simply allocating the values of subspace eigenvector components to every cable node that is associated with the basis vector in question, taking into account the correct signs of the basis-vector components as given by Eqs. (4) to (15). Since the conventional diagonal mass matrix $[\mathbf{M}]$ consists of identical elements m_{ii} ($=10$ kg), it means the $\{\mathbf{H}_i\}$ and $\{\mathbf{U}_i\}$ vectors in Eq. (51) are of identical form (except for a scalar multiplier), and so the system eigenvectors $\{\mathbf{U}_i\}$ may be taken as the actual deflection ordinates of the cable net.

Table 2 gives the 32 deflection ordinates of the three mode shapes of subspace $S^{(1)}$ in the full space of the problem, the modes being denoted by $\mathbf{U}_1^{(1)}$, $\mathbf{U}_2^{(1)}$ and $\mathbf{U}_3^{(1)}$. Ordinates of nodes of the top layer (1 to 16) appear in the upper part of the table; ordinates of nodes of the bottom layer (17 to 32) appear in the lower part. Positive values denote displacement towards the horizontal plane of symmetry of the cable net (i.e. downwards for top-layer nodes, and upwards for bottom-layer nodes). Table 3 gives the 32 deflection ordinates of the one mode shape of subspace $S^{(2)}$ in the full space of the problem, the mode being denoted by $\mathbf{U}_1^{(2)}$. These are either $+1$ or -1, depending on the sign of the basis-vector component of the node in question as given by Eq. (5); zero values denote nodes that do not participate in the motion (i.e. stationary nodes). Table 4 gives the 32 deflection ordinates of the four mode shapes of subspace $S^{(10A)}$ in the full space of the problem, the modes being denoted by $\mathbf{U}_1^{(10A)}$, $\mathbf{U}_2^{(10A)}$, $\mathbf{U}_3^{(10A)}$ and $\mathbf{U}_4^{(10A)}$. The results in Tables 2–4 are plotted in Figs. 14–16 respectively, where the displaced profiles of the cables are shown in red, and the vertical displacements of the nodes are shown by the blue lines. The plots allow visualisation of the vibration pattern of the modes; in regions where the position of the displaced cable net is not too clear, reference should be made to the values in the tables.

The results of this numerical study show that the 32 natural frequencies of the cable net occur in a relatively narrow band (from $f=0.098$ Hz to $f=0.377$ Hz). If external excitation forces also lie within this range, resonance may be avoided by increasing the tension in the cables or the stiffness of the inter-layer coupling, to increase the natural frequencies of the cable net beyond the

Table 4
Deflection ordinates of the four mode shapes of subspace $S^{(10A)}$ of the numerical example.

Node	1	2	3	4	5	6	7	8	9	10	11	12	13	14	15	16
$\mathbf{U}_1^{(10A)}$	1.00	1.12	0.50	0	1.12	1.00	0	−0.50	0.50	0	−1.00	−1.12	0	−0.50	−1.12	−1.00
$\mathbf{U}_2^{(10A)}$	1.00	0	−1.00	0	0	0	0	1.00	−1.00	0	0	0	0	1.00	0	−1.00
$\mathbf{U}_3^{(10A)}$	1.00	0	0	0	0	−1.00	0	0	0	0	1.00	0	0	0	0	−1.00
$\mathbf{U}_4^{(10A)}$	1.00	−1.12	0.50	0	−1.12	1.00	0	−0.50	0.50	0	−1.00	1.12	0	−0.50	1.12	−1.00

Node	17	18	19	20	21	22	23	24	25	26	27	28	29	30	31	32
$\mathbf{U}_1^{(10A)}$	1.00	1.12	0.50	0	1.12	1.00	0	−0.50	0.50	0	−1.00	−1.12	0	−0.50	−1.12	−1.00
$\mathbf{U}_2^{(10A)}$	1.00	0	−1.00	0	0	0	0	1.00	−1.00	0	0	0	0	1.00	0	−1.00
$\mathbf{U}_3^{(10A)}$	1.00	0	0	0	0	−1.00	0	0	0	0	1.00	0	0	0	0	−1.00
$\mathbf{U}_4^{(10A)}$	1.00	−1.12	0.50	0	−1.12	1.00	0	−0.50	0.50	0	−1.00	1.12	0	−0.50	1.12	−1.00

excitable range. Inter-layer damping may also be installed to control the vibrations. The numerical results also reveal the existence of modes of different symmetry type but having the same natural frequencies (compare: f_1 of subspace $S^{(1)}$ with f_1 of subspace $S^{(3)}$; f_1 of subspace $S^{(4)}$ with f_1 of subspace $S^{(2)}$; f_1 of subspace $S^{(7)}$ with f_1 of subspace $S^{(9)}$; f_1 of subspace $S^{(8)}$ with f_1 of subspace $S^{(6)}$) and modes of the same symmetry type having coincident natural frequencies (compare: f_2 and f_3 for subspaces $S^{(5A)}$ and $S^{(10A)}$). All these phenomena are consequencies of symmetry.

9. Summary and conclusions

The group-theoretic study of the vibration characteristics of double-layer cable nets of D_{4h} symmetry, commenced in a previous paper (Zingoni, 2018), has now been concluded. The first paper focussed on qualitative aspects of the problem, while the present paper has considered computational aspects. In the first paper, we used group theory to predict the type of symmetries which the vibration modes are going to have, the number of modes that will exhibit a given type of symmetry, the existence of pairs of modes of the same natural frequency, and the nature of the symmetry associated with such paired modes. By examining the dimensions of the various subspaces into which the original vector space of the problem decomposes, we also obtained a very good sense of the reduction in computational effort to be expected in performing the vibration analysis via the vector-space decomposition afforded by group theory.

In the present paper, we have presented the complete group-theoretic formulation of the vibration problem of the D_{4h} double-layer cable net. On the basis of the subspace basis vectors that were derived in the first paper, we have derived the equilibrium matrices for each subspace (i.e. the $B^{(\mu)}$ matrices) in explicit form, and shown how the symmetry-adapted flexibility matrices for the subspaces (i.e. the $A^{(\mu)}$ matrices) are obtained from the $B^{(\mu)}$ matrices. The assembly of the symmetry-adapted mass matrix for each subspace has also been explained. This has been followed by the formulation of the eigenvalue problem within the independent subspaces. The roots of the characteristic equation for a given subspace yields the eigenvalues of that subspace, which are a subset of the real eigenvalues of the original problem. Finally, the procedure for obtaining eigenvectors within the subspaces, and converting these into eigenvectors in the full vector space of the problem (i.e. actual mode shapes of the cable net), has been explained. The full computational procedure has been illustrated by consideration of a numerical example.

For the double-layer cable net of D_{4h} symmetry, the present study has revealed further insights on transverse-extension modes which do not exist in the case of a single-layer cable net of C_{4v} symmetry (Zingoni, 1996). The spring-like coupling between the two layers of the cable net permits the layers to move independently of each other, thus doubling the total number of system degrees of freedom, in comparison with single-layer cable nets. It is the occurrence of these additional transverse-extension modes (or "breathing" modes) that has distinguished the present study from previous work (Zingoni, 1996).

Thus, and by examination of the results of Section 5, we see that the $B^{(\mu)}$ matrices for subspaces $S^{(1)}$, $S^{(2)}$, $S^{(3)}$, $S^{(4)}$ and $S^{(10A)}$ feature the stiffness parameter k_i (i being 1, 2 or 3) associated with the coupling between the two layers of the cable net, and hence represent the transverse-extension modes of the cable net. On the other hand, the $B^{(\mu)}$ matrices for subspaces $S^{(5A)}$, $S^{(6)}$, $S^{(7)}$, $S^{(8)}$ and $S^{(9)}$ are independent of k_i, showing that the two layers move together in the same direction without relative separation, as if they were one layer. Thus these subspaces have modes (and natural frequencies) which are identical to those of the single-layer cable net.

Detailed consideration of a numerical example has illustrated the procedure for the calculation of eigenvalues and eigenvectors of the problem, hence natural frequencies and mode shapes of the cable net. The numerical results have revealed the existence of modes of different symmetry type that have the same natural frequencies, as well as modes of the same symmetry type that have coincident natural frequencies; all these phenomena are consequencies of symmetry.

For the problem in question, it has been shown how the group-theoretic procedure simplifies the determination of eigenvalues. Instead of tackling a 32 d.o.f. system and eventually having to solve a polynomial equation of degree 32, the group-theoretic approach has decomposed the problem into ten subspaces of smaller dimensions (the highest subspace dimension being only 4), which yield ten polynomial equations of smaller degree (the highest degree being only 4). This simplification represents a drastic reduction in computational effort. For double-layer cable nets that may be envisaged as long-span roofing solutions, or as deployable mesh reflector antennas for space applications (Li et al., 2013) (where the symmetry group D_{nh} is of higher order than D_{4h}, and the cable arrangement is more complex), the total number of nodes may be very large, making it more worthwhile to take advantage of a group-theoretic computational strategy.

References

Buchholdt, H.A., Davies, M., Hussey, M.J.L., 1968. The analysis of cable nets. J. Inst. Math. Appl. 4, 339–358.
Calladine, C.R., 1982. Modal stiffnesses of a pretensioned cable net. Int. J. Solids Struct. 18, 829–846.
Chen, Y., Feng, J., 2012. Generalized eigenvalue analysis of symmetric prestressed structures using group theory. J. Comput. Civil Eng. 26 (4), 488–497.
Chen, Y., Feng, J., 2016. Improved symmetry method for the mobility of regular structures using graph products. J. Struct. Eng. 142, 04016051.
Chen, Y., Feng, J., Ma, R., Zhang, Y., 2015a. Efficient symmetry method for calculating integral prestress modes of statically indeterminate cable-strut structures. J. Struct. Eng. 141 (10), 04014240.

Chen, Y., Sareh, P., Feng, J., 2015b. Effective insights into the geometric stability of symmetric skeletal structures under symmetric variations. Int. J. Solids Struct. 69/70, 277–290.
Chen, Y., Sareh, P., Feng, J., Sun, Q., 2017. A computational method for automated detection of engineering structures with cyclic symmetries. Comput. Struct. 191, 153–164.
Chen, Y., Fan, L., Feng, J., 2018. Automatic and exact symmetry recognition of structures exhibiting high-order symmetries. *J. Comput. Civ. Eng.* (ASCE) 32, 04018002.
Fowler, P.W., Guest, S.D., 2000. A symmetry extension of Maxwell's rule for rigidity of frames. Int. J. Solids Struct. 37 (12), 1793–1804.
Guest, S.D., Fowler, P.W., 2007. Symmetry conditions and finite mechanisms. J. Mech. Mater. Struct. 2 (2), 293–301.
Hamermesh, M., 1962. Group Theory and Its Application to Physical Problems. Pergamon Press, Oxford.
Harth, P., Michelberger, P., 2016. Determination of loads in quasi-symmetric structure with symmetry components. Eng. Struct. 123, 395–407.
Healey, T.J., Treacy, J.A., 1991. Exact block diagonalisation of large eigenvalue problems for structures with symmetry. Int. J. Numer. Methods Eng. 31, 265–285.
Healey, T.J., 1988. A group-theoretic approach to computational bifurcation problems with symmetry. Comput. Methods Appl. Mech. Eng. 67, 257–295.
Ikeda, K., Murota, K., 1991. Bifurcation analysis of symmetric structures using block--diagonalisation. Comput. Methods Appl. Mech. Eng. 86, 215–243.
Irvine, H.M., 1981. Cable Structures. MIT Press, Cambridge Massachusetts.
Kangwai, R.D., Guest, S.D., 1999. Detection of finite mechanisms in symmetric structures. Int. J. Solids Struct. 36, 5507–5527.
Kangwai, R.D., Guest, S.D, 2000. Symmetry-adapted equilibrium matrices. Int. J. Solids Struct. 37, 1525–1548.
Kangwai, R.D., Guest, S.D., Pellegrino, S., 1999. An introduction to the analysis of symmetric structures. Comput. Struct. 71, 671–688.
Kaveh, A., Jahanmohammadi, A., 2008. Group-theoretic method for forced vibration analysis of symmetric structures. Acta Mech. 199, 1–16.
Kaveh, A., Koohestani, K., 2008. Graph products for configuration processing of space structures. Comput. Struct. 86, 1219–1231.
Kaveh, A., Nikbakht, M., 2007. Decomposition of symmetric mass-spring vibrating systems using groups, graphs and linear algebra. Commun. Numer. Methods Eng. 23, 639–664.
Kaveh, A., Nikbakht, M., 2010. Improved group-theoretical method for eigenvalue problems of special symmetric structures using graph theory. Adv. Eng. Softw. 41, 22–31.
Kaveh, A., Rahami, H., 2004. An efficient method for decomposition of regular structures using graph products. Int. J. Numer. Methods Eng. 61 (11), 1797–1808.
Li, T.J., Jiang, J., Deng, H.Q., Lin, Z.C., Wang, Z.W., 2013. Form-finding methods for deployable mesh reflector antennas. Chin. J. Aeronaut. 26 (5), 1276–1282.
Mohan, S.J., Pratap, R., 2002. A group theoretic approach to the linear free vibration analysis of shells with dihedral symmetry. J. Sound Vib. 252, 317–341.
Mohan, S.J., Pratap, R., 2004. A natural classification of vibration modes of polygonal ducts based on group theoretic analysis. J. Sound Vib. 269, 745–764.
Otto, F. (Ed.), 1966. Tensile Structures. MIT Press, CambridgeMassachusetts.
Pellegrino, S., Calladine, C.R., 1984. Two-step matrix analysis of prestressed cable nets. In: Proceedings of the Third International Conference on Space Structures, pp. 744–749.
Schonland, D., 1965. Molecular Symmetry. Van Nostrand, London.
Siev, A., 1963. A general analysis of prestressed nets. Publ. Int. Assoc. Bridge Struct. Eng. 23, 283–292.
Suresh, K., Sirpotdar, A., 2006. Automated symmetry exploitation in engineering analysis. Eng. Comput. 21 (4), 304–311.
Szabo, J., Kollar, L., 1984. Structural Design of Cable-Suspended Roofs. Akademiai Kiado, Budapest.
Vilnay, O., Rogers, P., 1990. Statical and dynamical response of cable nets. Int. J. Solids Struct. 26, 299–312.
Vilnay, O., 1990. Cable Nets and Tensegric Shells. Ellis Horwood, Chichester.
Weyl, H., 1932. Theory of Groups and Quantum Mechanics. Dover Publications, New York.
Wigner, E.P., 1959. Group Theory and Its Applications to the Quantum Mechanics of Atomic Spectra. Academic Press, New York.
Zingoni, A., Pavlovic, M.N., Zlokovic, G.M., 1995a. A symmetry-adapted flexibility approach for multi-storey space frames: general outline and symmetry-adapted redundants. Struct. Eng. Rev. 7, 107–119.
Zingoni, A., Pavlovic, M.N., Zlokovic, G.M., 1995b. A symmetry-adapted flexibility approach for multi-storey space frames: symmetry-adapted loads. Struct. Eng. Rev. 7, 121–130.
Zingoni, A., 1996a. An efficient computational scheme for the vibration analysis of high-tension cable nets. J. Sound Vib. 189 (1), 55–79.
Zingoni, A, 1996b. Truss and beam finite elements revisited: a derivation based on displacement-field decomposition. Int. J. Space Struct. 11 (4), 371–380.
Zingoni, A., 2005a. On the symmetries and vibration modes of layered space grids. Eng. Struct. 27 (4), 629–638.
Zingoni, A., 2005b. A group-theoretic formulation for symmetric finite elements. Finite Elem. Anal. Des. 41 (6), 615–635.
Zingoni, A., 2008. On group-theoretic computation of natural frequencies for spring–mass dynamic systems with rectilinear motion. Commun. Numer. Methods Eng. 24, 973–987.
Zingoni, A., 2009. Group-theoretic exploitations of symmetry in computational solid and structural mechanics. Int. J. Numer. Methods Eng. 79, 253–289.
Zingoni, A., 2012a. A group-theoretic finite-difference formulation for plate eigenvalue problems. Comput. Struct. 112/113, 266–282.
Zingoni, A., 2012b. Symmetry recognition in group-theoretic computational schemes for complex structural systems. Comput. Struct. 94/95, 34–44.
Zingoni, A., 2014. Group-theoretic insights on the vibration of symmetric structures in engineering. Philos. Trans. R. Soc. A 372, 20120037.
Zingoni, A., 2015. Vibration Analysis and Structural Dynamics for Civil Engineers: Essentials and Group-Theoretic Formulations. CRC Press/Taylor and Francis, London.
Zingoni, A., 2018. Insights on the vibration characteristics of double-layer cable nets of D_{4h} symmetry. Int. J. Solids Struct. 135, 261–273.
Zlokovic, G.M., 1989. Group Theory and G-Vector Spaces in Structural Analysis. Ellis Horwood, Chichester.